Methods[1]

Expedition 308 Scientists[2]

Chapter contents

Introduction to Expedition 308 shipboard methods

The "Methods" chapter is designed to document the primary procedures and methods employed during Expedition 308 by the scientists in the various shipboard laboratories in order to understand the basis for our preliminary interpretations of the core and logging data. This information concerns only shipboard methods, the results of which are presented in the site reports in the "Expedition reports" section of the Expedition 308 *Proceedings of the Integrated Ocean Drilling Program* volume. Methods for shore-based analysis of Expedition 308 samples and data will be described in the individual scientific contributions to be published in scientific journals and the "Research results" section of the Expedition 308 *Proceedings* volume.

Operations

Two standard coring systems were used during Expedition 308: the advanced piston corer (APC) and the extended core barrel (XCB) systems. These standard coring systems and their characteristics are summarized in the "Explanatory Notes" chapters of previous *Initial Reports* volumes of the Ocean Drilling Program (ODP). The Leg 139 *Initial Reports* volume includes a particularly detailed description (Davis, Mottl, Fisher, et al., 1992), as does a variety of ODP *Technical Notes* (**www-odp.tamu.edu/publications/pubs_tn.htm**). Additional measurement-while-drilling (MWD) and logging-while-drilling (LWD) tools deployed during Expedition 308 are described in detail in **"Downhole measurements."**

Drilled intervals are measured from the Kelly bushing on the rig floor to the bottom of the drill pipe and referred to in meters below rig floor (mbrf). Meters below seafloor (mbsf) references for the core tops are calculated by subtracting the seafloor depth. When sediments of substantial thickness cover the seafloor, the mbrf depth of the seafloor is determined with a mudline core, assuming 100% recovery for the cored interval in the first partly filled core barrel. Water depth is calculated by subtracting the distance from the rig floor to sea level from the mudline measurement in mbrf. This water depth usually differs from precision depth recorder measurements by a few to several meters.

[1]Expedition 308 Scientists, 2006. Methods. *In* Flemings, P.B., Behrmann, J.H., John, C.M., and the Expedition 308 Scientists, *Proc. IODP,* 308: College Station TX (Integrated Ocean Drilling Program Management International, Inc.). doi:10.2204/iodp.proc.308.102.2006
[2]**Expedition 308 Scientists' addresses.**

doi:10.2204/iodp.proc.308.102.2006

Core handling and shipboard analysis

As soon as cores arrived on deck, gas void samples and headspace samples were taken by means of a syringe, if applicable, for immediate analysis as part of the shipboard safety and pollution prevention program. Core catcher samples were taken for biostratigraphic analysis. When the core was cut in sections, whole-round samples were taken for shipboard interstitial water examinations and microbiology analysis (both shipboard and shore based).

Before splitting, whole-round core sections not dedicated to microbiology were run through the multisensor track (MST), and thermal conductivity measurements were taken. Whole-round samples dedicated to geotechnical analysis were then taken. Finally, the cores were split into working and archive halves, from bottom to top, so investigators should be aware that older material could have been transported upward on the split face of each section. The working half of each core was sampled for both shipboard analyses, such as physical properties, carbonate, and X-ray diffraction (XRD) mineralogy, and shore-based studies. The archive halves were photographed with both black-and-white and color film, scanned with the digital imaging system (DIS), described visually and by means of smear slides, measured for color reflectance on the archive-half multisensor track (AMST), and run through the cryogenic magnetometer. Close-up photographs were taken of particular features for illustrations in site summary reports, as requested by scientists.

Both halves of the core were then put into labeled plastic tubes, sealed, and transferred to cold storage space aboard the ship. At the end of the expedition, the cores were transferred from the ship to cold storage at the Integrated Ocean Drilling Program (IODP) Gulf Coast Core Repository at Texas A&M University in College Station, Texas.

Curatorial procedures and sample depth calculations

Numbering of sites, holes, cores, and samples follows the standard IODP procedure. A full curatorial identifier for a sample consists of the expedition, site, hole, core number, core type, section number, and interval in centimeters measured from the top of the core section. For example, a sample identification of 308-U1319A-1H-1, 10–12 cm, represents a sample removed from the interval between 10 and 12 cm below the top of Section 1, Core 1 of Hole U1319A during Expedition 308 (H designates that this core was taken with the APC system [X = XCB]). Cored intervals are also referred to in "curatorial" mbsf. The mbsf depth of a sample is calculated by adding the depth of the sample below the section top and the lengths of all higher sections in the core to the core-top datum measured with the drill string.

A sediment core from less than a few hundred mbsf may, in some cases, expand upon recovery (typically 10% in the upper 300 m), in which case its length will not match the drilled interval. In addition, a coring gap typically occurs between cores, as shown by composite depth construction (see the "Explanatory Notes" chapters for Legs 138, 177, and 184 [Shipboard Scientific Party, 1992, 1999, 2000]). Thus, a discrepancy may exist between the drilling mbsf and the curatorial mbsf. For instance, the curatorial depth (mbsf) of a sample taken from the bottom of a core may be larger than that of a sample from the top of the subsequent core. During Expedition 308, multiple APC/XCB holes were cored but continuous composite sections were not constructed.

If a core has incomplete recovery, all cored material is assumed to originate from the top of the drilled interval as a continuous section for curation purposes. The true depth interval within the cored interval is not known, resulting in an uncertainty, for instance, in age-depth analysis and correlation of core facies with downhole log signals.

Lithostratigraphy

The techniques and procedures used to describe, analyze, and name the lithologies recovered during Expedition 308 are detailed below and follow ODP *Technical Note* 8 (Mazzullo and Graham, 1988). These include visual core descriptions (VCDs), smear slide and thin section descriptions, XRD analyses, color spectrophotometry, and high-resolution digital color imaging. Any significant deviations from the procedures outlined in this section are discussed in the individual site chapters.

Sediment classification

Principal names were assigned to sediments based on composition, texture, and degree of lithification as determined primarily from visual description and smear slide analyses. Modifiers to the principal name were determined based on both the abundance and type of the nonprincipal component or components (e.g., siliciclastic or biogenic). Total inorganic carbon content, including calcium carbonate, of the sediments (see "Solid-phase chemistry" in "Geochemistry and microbiology" in the "Site U1319," "Site U1320," "Site U1322," and "Site U1324" chapters) was also used to aid in classifying sediments. Major modifiers, those components that form >25% of the sediment, precede the principal name and are listed in order of increasing abundance. Genetic terms,

such as "pelagic," "neritic," "turbidite," and "debris flow," were not used in classifying the sediments and are used only in geologic interpretations of the sedimentary unit. The conventions used here were applied only to granular sediments. Chemical sediments were only encountered as accessory minerals and nodules.

Siliciclastic sediments

For sediments and rocks composed of >60% siliciclastic components, the principal name was determined by the size of the grains, derived from the Udden-Wentworth grain-size scale (Wentworth, 1922) (Fig. **F1**). In this classification scheme, the term "clay" is independent of mineralogy and refers to all siliciclastic grains <3.9 µm in size. The relative proportion of different grain sizes was determined by visual percentage estimation using a standard comparison chart with half-ϕ unit intervals (e.g., Terry and Chilingar, 1955). Where possible in sand beds, the modifiers "upper" and "lower" are used to describe whether the sediment is predominantly in the upper half or lower half of an individual ϕ-size class (e.g., medium upper sand for grains with a typical size between 1.5ϕ and 1ϕ). For silt and clays, the grain size was estimated using smear slides. Once the relative proportion of the various grain sizes was estimated, a modified Shepard (1954) classification scheme was used to modify, if necessary, the principal name using the ternary diagram in Figure **F2.** Clay, silt, and sand are the principal names in the diagram. If either the silt or sand component exceeds 25% of the total siliciclastic grains, it becomes a modifier to the principal name. For example, sediment composed of 10% clay and 90% silt is simply silt, whereas sediment composed of 30% silt and 70% sand is silty sand. Where the proportions of silt and clay were difficult to quantify, the term "mud" was used for sediment containing mixtures of clay and silt.

Where diagnostic minerals (e.g., glauconite), biogenic sediments (e.g., foraminifers), or unusual components (e.g., volcanic glass) compose ≥5% of the sediment, the naming conventions of biogenic and mixed sediments were adopted. Thus, if the mineral component represents between 5% and 10% of the sediment, it is hyphenated with the suffix "-bearing" and precedes the major siliciclastic component name. If the component is 10%–40% of the sediment, it is hyphenated with the suffix "-rich" instead. For example, sediment composed of 15% sand-sized foraminifer tests, 30% silt, and 55% clay is called a foraminifer-rich silty clay. Where volcanic glass composed >40% of the sedimentary components, the name volcanic ash was used.

Biogenic sediments

Unlike siliciclastic sediments, biogenic sediments, defined as containing >60% biogenic components, are not described based on grain size. Rather, the principal name for all biogenic sediments is ooze. If the siliciclastic component represents 5%–40% of a sediment, the naming conventions using "-rich" and "-bearing" as described for mixed sediments below are used. Thus, a sediment composed of 30% siliciclastic clay and 70% sand-sized foraminifers is called a clay-rich foraminifer ooze, not a clay-rich foraminifer sand.

Mixed sediments

Mixtures of biogenic and nonbiogenic material, where the biogenic content is 40%–60%, are termed "mixed sediments" (Mazzullo and Graham, 1988). The name of a mixed sediment consists of a major modifier(s) consisting of the name(s) of the major fossil group(s), with the least common fossil listed first, followed by the principal name appropriate for the siliciclastic components (e.g., foraminifer clay). The same naming conventions for using "-bearing" and "-rich" apply to mixed sediments as described above. Sediment containing 5% foraminifers, 40% nannofossils, and 55% silt is, thus, called foraminifer-bearing nannofossil silt. Sediment containing 5% diatoms, 40% clay, and 55% nannofossils is called diatom-bearing nannofossil clay.

Visual core descriptions

Detailed sedimentologic observations and descriptions were recorded manually for each core section on paper (barrel sheets). A variety of features that characterize the sediments were recorded, including lithology, sedimentary structures, color, diagenetic precipitates, and core disturbance. Compositional data were obtained from smear slides. The color of the sediments was determined first by visual observation at the description table and then quantitatively by color spectrophotometry using the AMST. This information was then transcribed into VCD forms using AppleCORE software (version 9.4a), which generated a one-page graphical description of each core. An example of such a VCD from Expedition 308 is shown in Figure **F3.** The legend for the symbols used for lithology, sedimentary structures, and other features seen in Expedition 308 cores are explained in Figure **F4.** The VCD forms are available digitally in the core descriptions, and the scanned barrel sheets are available upon request.

Lithology and grain size

Lithology and grain size of the described sediments are represented graphically in a column on the VCD

using the symbols illustrated in Figure F4. A maximum of three different lithologies (for interbedded sediments) or three different components (for mixed sediments) can be represented within the same core interval using AppleCORE software. Intervals that are a few centimeters thick or thicker can be portrayed accurately in the Lithology column. Percentages are rounded to the nearest 10%, and lithologies that constitute <10% of the core are generally not shown but are listed in the Description column.

Sedimentary structures

Each type of sedimentary structure and its exact location are displayed in the Structure column of the VCD (Fig. F3). Symbols used for sedimentary structures encountered throughout Expedition 308 are listed in Figure F4. Some of the more common structures and accessories observed were parallel laminations, climbing ripples, graded bedding, mud clasts, contorted beds, wood fragments, plant debris, and mottling.

Fossils

The presence of macroscopic fossils such as shell fragments and preserved whole shells were identified whenever possible and displayed in a separate column on the barrel sheet.

Sediment disturbance

Drilling-related sediment disturbance is recorded in the Disturbance column on the VCD (Fig. F3). Separate terms are used to describe the degree of drilling disturbance:

- Slightly disturbed = bedding contacts are slightly deformed.
- Moderately disturbed = bedding contacts have undergone extreme bowing.
- Highly disturbed = bedding is completely deformed as flow-in, coring/drilling slough, and other soft-sediment stretching and/or compressional shearing structures attributed to coring/drilling (e.g., gas expansion).
- Soupy = intervals are water saturated and have lost all primary sedimentary structures.
- Drilling biscuits = drilling slurry surrounding an intact or slightly fractured drilling biscuit, usually associated with XCB coring.

Cores recovered from gas-bearing sediments are often disturbed by gas expansion and fracturing as they are brought to surface conditions. In cases where it is possible to distinguish between disturbance of the core resulting from drilling and disturbance resulting from gas expansion, notes were made in the Comments section of the barrel sheet listing the depths at which gas fracturing was observed.

Samples

The locations of samples are indicated in the Sample column on the VCD. The abbreviations used are as follows:

SmS = smear slide.
IW = interstitial water.
MBI/BIO = microbiology.
PAL = micropaleontology.
WHC = whole-round core.

Smear slide analyses

Smear slides were prepared from the archive halves of the cores. With a toothpick, a small amount of sediment was taken and put on a 2.5 cm × 7.5 cm glass slide, homogenized, and dispersed over the slide with a drop of deionized water. The sample was then dried on a hot plate at a low temperature. A drop of Norland optical adhesive and a 2.5 cm × 2.5 cm cover glass were added. The smear slide was fixed in an ultraviolet light box. With a transmitted-light petrographic microscope, both the grain size and abundance of dominant components in a sample were determined. Abundance was estimated with the help of a comparison chart for visual percentage estimation (after Terry and Chilingar, 1955). Note that smear slide analyses tend to underestimate the amount of sand-sized and larger grains because these grains are difficult to incorporate into the slide. The smear slide results are available from the IODP database, and the tables include information about the location of samples, their grain-size distribution, and whether the sample represents the dominant or the minor lithology in the core. Additionally, it provides estimates of the major mineralogical and biological components from the examination of each smear slide. The presence of authigenic minerals, such as manganese oxides, iron sulfides, or carbonates, as well as the presence of rare trace minerals, was noted in the Comments column. The mineralogy of the major smear slide components was also validated by XRD analysis, and the relative proportion of carbonate and noncarbonate material was validated by chemical analysis of the sediments (see "Solid-phase chemistry" in "Geochemistry and microbiology" in the "Site U1319," "Site U1320," "Site U1322," and "Site U1324" chapters).

X-ray diffraction analyses

XRD analyses were used to support and verify smear slide descriptions. Each sample was freeze-dried,

ground, and mounted with a random orientation into an aluminum sample holder. For these measurements, a Philips PW-1729 X-ray diffractometer with a CuK_α source (40 kV and 35 mA) and a Ni filter was used. Peak intensities were converted to values appropriate for a fixed slit width. The goniometer scan was performed from 2°2θ to 70°2θ at a scan rate of 1.2°/min (step = 0.01° and count time = 0.5 s). Diffractograms were peak-corrected to match the (100) quartz peak at 4.26 Å. Common minerals were identified based on their peak position and relative intensities in the diffractogram using the software package MacDiff (version 4.2.5; **www.pangaea.de/Software**).

Color reflectance spectrophotometry

In addition to visual estimates of color, reflectance of visible light from soft sediment was measured using a Minolta spectrophotometer (model CM-2002) mounted on the AMST. The AMST measures the archive half of each core section and provides point measurements of downcore color variations for the visible wavelengths (400–700 nm). Freshly split cores were covered with clear plastic wrap and placed on the AMST. The AMST skips empty intervals and intervals where the core surface is well below the level of the core liner but does not recognize relatively small cracks or disturbed areas of core. Thus, AMST data may contain spurious measurements that should be edited out of the data set before use. Each measurement consists of 31 separate determinations of reflectance in 10 nm wide spectral bands from 400 to 700 nm. Additional detailed information about the measurement and interpretation of spectral data with the Minolta spectrophotometer can be found in Balsam et al. (1997, 1998) and Balsam and Damuth (2000). The AMST was also used to acquire point magnetic susceptibility measurements (see **"Paleomagnetism"**). Color reflectance and magnetic susceptibility measurements were useful to distinguish turbidites and hemipelagic sediments.

Digital color imaging

All core sections were imaged using the Geotek X-Y DIS soon after being split and scraped. Scraping the cores immediately prior to imaging helped capture ephemeral sedimentary features, particularly faint color banding and laminations, which often become oxidized within minutes of core splitting. Core sections were routinely loaded into each imaging tray of the DIS as soon as the previous sections were imaged so that the imaging system ran continuously during section loading and unloading. Digital images were displayed after scanning to ensure they were stored.

All images were acquired at a crosscore and downcore resolution of 100 pixels/cm. At the beginning of Expedition 308, the acquisition aperture was varied in an attempt to maximize the dynamic range captured. The barcode label and the polystyrene inserts (e.g., for voids and whole-round samples) were placed at the end of each section. Output from the DIS includes an uncompressed TIFF file (available upon request) and a compressed Mr.Sid (.sid) file (available in the **Janus** database) for each scanned section. Red-green-blue (RGB) profiles for all images were also automatically saved (available upon request) but were generally not used on board. Additional postprocessing of the color imagery was done to achieve a "medium"-resolution JPEG (.jpg) image of each section and a composite PDF (.pdf) image of each core.

In addition to the DIS scanning of the core sections, whole-core photographs were acquired with a large-format color camera. The photographs took place between 30 and 60 min after the core was scraped. Consequently, some of the sedimentary details may be lost using the more conventional archive-core table photographs. For this reason, cores were scraped before close-up digital photographs were taken.

Biostratigraphy

During Expedition 308, calcareous nannofossils and foraminifers were examined for age dating of samples taken primarily from core catchers. Chronobiostratigraphy was mainly based on the zonation scheme of Berggren et al. (1995) (Fig. **F5**). As most drilling activities were on late Quaternary sequences, local species datums and zonations based on species abundance such as those of Kennett and Huddlestun (1972) were also used. Ages for assemblage zonal boundaries were adjusted to marine isotope stages (MIS) given in Bassinot et al. (1994).

Calcareous nannofossils

Zonation and taxonomic concept

We have referred primarily to the zonation and code of Hine and Weaver (1998) (Fig. **F6**) for dating the cored sediments. We followed taxonomic concepts summarized in Perch-Nielsen (1985).

Methods

Standard smear slides were prepared for all samples using Norland optical adhesive as a mounting medium.

Assemblages of calcareous nannofossils were studied from smear slides prepared for each core catcher

sample and a few samples from selected cores. In the latter case, hemipelagic and pelagic beds were sampled in order to avoid effects of resedimentation resulting from turbidites and mass transport deposits (MTDs), and special attention was given to lithologic changes. Examination was done exclusively with a transmitted light microscope, and a magnification of 1000× was used to estimate relative abundances.

We used Bugwin (version 2002.3.8) software for collecting and analyzing nannofossil data. BugCam software, specifically designed by the University of Florida, was used for taxa identification. All species were counted within 10 fields of view. Abundance of individual species is reported on the basis of 100 fields of view. On collecting data the species distribution charts were created and analyzed.

Individual species abundances were determined as follows:

Rare = 1–3 specimens/100 fields of view (FOV).
Sparse = 4–10 specimens/100 FOV.
Frequent = 11–25 specimens/100 FOV.
Frequent–common = 26–100 specimens/100 FOV.
Common = 101–500 specimens/100 FOV.
Abundant = 501–1000 specimens/100 FOV.
Very abundant = 1001–10,000 specimens/100 FOV.
Ooze = >10,000 specimens/100 FOV.

The total abundance of calcareous nannofossils for each sample was estimated as follows:

B = barren.
R = rare (<100 specimens/100 FOV [half of a traverse]).
F = frequent (100–500 specimens/100 FOV).
C = common (501–1000 specimens/100 FOV).
A = abundant (1001–10,000 specimens/100 FOV).
W = very abundant (>10,000 specimens/100 FOV).

The preservation of calcareous nannofossils was classified as good, moderate, or poor. These categories represent subjective impressions with the following definitions:

P = poor (strong and severe dissolution, overgrowth, and/or fragmentation has occurred; primary diagnostic features may have been destroyed, impossible to identify many specimens at the species level).
M = moderate (dissolution and/or overgrowth are evident; a significant proportion [as much as 25%] of the specimens cannot be confidently identified at the species level with absolute certainty).
G = good (evidence of dissolution and/or overgrowth is very little; diagnostic characteristics are preserved nearly in all nannofossils; ~95% of all specimens or more can be identified).

Foraminifers

Methods

Samples of ~40 cm^3 were soaked in a Calgon solution and washed through a 63 µm sieve. Samples were rinsed and then dried under a heat lamp or in an oven at 60°C.

Preservation characteristics were divided into four categories:

P = poor (almost all specimens were dissolved or broken and fragments dominated).
M = moderate (30%–60% of specimens showed dissolved or broken chambers).
G = good (61%–90% of specimens were well preserved and unbroken).
VG = very good (>90% of specimens were well preserved and unbroken).

Planktonic foraminifers

The >125 µm size fraction was examined for planktonic foraminifers and the 63–125 µm size fraction was studied for zonal markers if these were absent in the larger size fractions.

The abundance of planktonic foraminifers is defined as follows:

B = barren.
T = trace (1 or 2 specimens).
VR = very rare (3–10 specimens).
R = rare (11–30 specimens).
F = frequent (31–100 specimens).
C = common (101–500 specimens).
A = abundant (>500 specimens).

We mainly referred to Bolli and Saunders (1985) for planktonic foraminifer taxonomy. The zonal scheme and species datum levels of Berggren et al. (1995) were used for dating major stratigraphic boundaries (Fig. **F5**). The planktonic foraminifer assemblage zones based on *Globorotalia menardii* for subdividing the late Quaternary in the Gulf of Mexico region (Kennett and Huddlestun, 1972; Martin et al., 1990) (Fig. **F7**) were also attempted when time allowed. Ages for these assemblage zone boundaries were modified according to the timescale of Bassinot et al. (1994).

Benthic foraminifers

Benthic foraminifer relative abundance was defined as follows:

B = barren.
R = rare (<1% of the fauna).
F = frequent (1%–5% of the fauna).
C = common (6%–20% of the fauna).
A = abundant (>20% of the fauna).

Benthic foraminifers were examined from the >63 µm size fraction. Paleobathymetry estimates were primarily based on Poag (1981) and van Morkhoven et al. (1986). Bathymetric zones were defined as follows:

Neritic = 0–200 m.
Upper bathyal = 200–600 m.
Middle bathyal = 600–1000 m.
Lower bathyal = 1000–2000 m.
Abyssal = >2000 m.

Paleomagnetism

Magnetic measurements

Paleomagnetic and rock magnetic measurements during Expedition 308 included natural remanent magnetization (NRM) and volume magnetic susceptibility (κ), both performed on continuous archive-half core sections.

NRM was measured on board at 5 cm intervals using an automated pass-through cryogenic direct-current (DC) superconducting quantum interference device (SQUID) rock magnetometer (2G Enterprises model 760-R) with an in-line alternating-field (AF) demagnetizer (model 2G600). The archive-half sections were demagnetized in 0, 10, 20, and, in some cases, 30 mT AF field increments (for details see "Paleomagnetism" in the site chapters). The pass-through cryogenic magnetometer and AF demagnetizer are controlled by 2G LongCore Labview software (version 207.3) (Shipboard Scientific Party, 2004).

NRM intensity, declination, direction, and inclination were measured. For the latter two parameters, a core orientation correction was applied using the digital multishot tool (Tensor, Inc.), which is rigidly mounted onto a nonmagnetic sinker bar during APC coring. The Tensor tool consists of three mutually perpendicular magnetic field sensors and two perpendicular gravity sensors. The information from both sets of sensors allows the azimuth and dip of the hole to be measured as well as the azimuth of the APC core double orientation line. The IODP core orientation scheme designates the positive x-axis direction as the horizontal (in situ) line radiating from the center of the core through the space between the double line scribed lengthwise on the working half of each core liner.

Volume magnetic susceptibility measurements were carried out at 1–6 cm resolution on whole-core sections as part of the MST analyses (see **"Physical properties"**). On the archive-half sections, the AMST analyzed color reflectance at 10 cm resolution (see **"Lithostratigraphy"**) and additional point magnetic susceptibility at 5–10 cm resolution using a Bartington MS2F sensor at a sensitivity setting of 0.1 instrument units. The instrument automatically zeroes and records a free-air value for the magnetic susceptibility at the start and end of each section run. Instrument drift during a section run is then corrected by subtraction of a linear interpolation between the first and last free-air measurements (Shipboard Scientific Party, 2003).

Magnetostratigraphy

Classical magnetostratigraphy using field reversal correlations (e.g., Cande and Kent, 1992) could not be used to establish an age model because the Brunhes/Matuyama Chron boundary was not recovered due to high sedimentation rates.

Instead, we used high-resolution variations of the Earth's magnetic field such as changes in declination and inclination. High-resolution rock magnetic records such as NRM intensity and magnetic susceptibility were potentially helpful tools for multiparameter correlations. Such rock magnetic records are capable of exhibiting Milankovitch cyclicities, sometimes in close agreement with $\delta^{18}O$ profiles. This correlation is generally explained by climatic impact on fluxes of magnetically enriched terrigenous and nonmagnetic biogenic or siliciclastic sedimentary components. Paleoclimatic signatures of magnetic susceptibility and various remanence parameters (such as NRM) are increasingly employed for high-resolution core correlation and have been described and used as stratigraphic correlation tools in paleoceanographic studies from all major oceans (e.g., Radhakrishnamurty et al., 1968; Kent, 1982; Robinson, 1986; Bloemendahl et al., 1988; deMenocal et al., 1991; Bickert et al., 1997; von Dobeneck and Schmieder, 1999). Frederichs et al. (1999) outlined the physical and sedimentological principles of rock magnetic climate proxies.

For marine sediments, κ may vary from an absolute minimum of -15×10^{-6} SI (diamagnetic minerals such as pure carbonates or silicates) to a maximum of ~10.000 × 10^{-6} SI for basaltic debris rich in (titano)magnetite. In most cases, κ is primarily determined by the concentration of ferrimagnetic minerals, whereas paramagnetic components such as clays are of minor importance. Enhanced susceptibilties indicate higher concentrations of lithogenic or authigenic ferrimagnetic components. This relation may serve for correlating sedimentary sequences deposited under similar global or regional conditions.

NRM intensity and κ were further compared with the sediment bulk density to perform multiparameter correlation of the rock magnetic shipboard data. Using these multiple logs is suitable to establish a re-

gional stratigraphic correlation and tentatively derive preliminary age estimates. Correlations are attempted by comparing the individual peaks and troughs of the records and constraining the tie points. These magnetostratigraphic tie points (referred to as "MTP") were then, if possible, correlated to the $\delta^{18}O$ record published by Bassinot et al. (1994). This provided the basis to establish a rough initial chronology and detect Milankovitch cyclicity.

Geochemistry and microbiology

Inorganic geochemistry

Whole-round pore water sample collection

Shipboard analyses were performed on interstitial waters extracted from 5 cm long whole-round sediment samples. Samples were collected every 1.5 m to the estimated base of the sulfate reduction zone at 50 mbsf. Below 50 mbsf, whole rounds were collected every 10 m to terminal depth (TD). The higher sampling frequency above 50 mbsf provided a better definition of the sulfate/methane interface (SMI). The whole-round sections were cut from the core immediately after recovery on deck. The surfaces of the samples were scraped with a polytetrafluoroethylene (PTFE)-coated spatula to remove sediment potentially contaminated with drilling fluids. Interstitial water was extracted by applying up to 40,000 lb of pressure in a titanium squeezer. The pore water samples were collected directly into a 60 mL plastic syringe, and sample splits were filtered through a 0.45 µm filter. The pore water volume extracted was ~40 mL. Whole-round intervals were increased to 10 cm long when pore water recovery was not sufficient to provide the volume required for analysis. Sample splits were sealed in plastic vials for shipboard analysis, IODP archives, and for shore-based elemental and isotopic analysis.

Rhyzon sample collection

High-resolution pore water sampling was conducted on the upper 15 m of selected holes using soil moisture probes called Rhyzon samplers. Rhyzon samplers enable discrete sampling with minimal disturbance to the sediment surface. The method does not require filtering or removal of wet sediment from the piston core. Rhyzon samplers used during Expedition 308 were 2.5 mm wide × 30 mm long filters with a pore size of 1 µM. The use of Rhyzon samplers to extract pore waters from marine sediments is potentially a powerful and novel alternative to the technique of squeezing whole-round sediments.

Samplers were inserted into the sediment at ~10 cm intervals. Pore water was withdrawn under vacuum into acid-washed 60 mL syringes or He-purged headspace vials. Whole-round cores were sampled prior to splitting for sedimentological description. Shipboard samples were stored in plastic vials in a refrigerator prior to analysis. Sediment samples were also collected for physical property testing including permeability and porosity. MST scans (see **"Physical properties"**) were run before and after sampling to assess potential alteration of sediment properties (see "Rhyzon" in **"Supplementary material"**).

Shipboard analyses

Interstitial water samples were analyzed for routine shipboard measurements according to standard procedures and calibrated against International Association of the Physical Sciences of the Oceans (IAPSO) standards (Gieskes et al., 1991). Alkalinity and pH were determined immediately following sample collection using the Metrohm autotitrator with a Brinkman combination pH electrode. The electrode was calibrated before the analyses and was checked periodically for drift. Salinity was estimated using an Index Instruments digital refractometer to measure the total dissolved solids. Chlorinity was determined by titration with silver nitrate. Concentrations of anions (SO_4^{2-} and Cl^-) and cations (Ca^{2+}, Mg^{2+}, K^+, and Na^+) were determined in duplicate using a Dionex ion chromatograph. All samples were run at 1:200 dilution. Standards were measured at the start and end of each run to test for drift in the response of the conductivity detector. Precision on separate dilutions was better than 2%. Concentrations of NH_4^+ and PO_4^{3-} were determined using a Milton Roy spectrophotometer. Minor element concentrations (Fe^{2+}, Mn^{2+}, Li^+, B^{3+}, Si^{2+}, Sr^{2+}, and Ba^{2+}) were analyzed using a JY2000 inductively coupled plasma–atomic emission spectrometer (ICP-AES) run at 1:10 dilution. Dissolved inorganic carbon (DIC) content was determined by coulometry.

Total inorganic carbon (TIC) content of the sediment was determined by coulometry. Total carbon (TC), nitrogen, and hydrogen sediment concentrations were determined with a Carlo Erba NCS analyzer. Total organic carbon (TOC) content was calculated as the difference between TC and TIC, where

$$TOC = TC - TIC.$$

Total sulfur analyses were inaccurate and of poor precision. These results were considered qualitative and are not reported.

Sample collection for shore-based analyses

Pore water splits were collected from whole-round interstitial water samples for shore-based elemental (minor and trace metal constituents) and isotopic

($\delta^{13}C$, $\delta^{15}N$, $\delta^{18}O$, δD, $\delta^{34}S$, $\delta^{11}B$, and $^{87}Sr/^{86}Sr$) analyses. Samples for elemental analysis were acidified with ultrapure HNO_3, whereas samples for isotopic analysis were preserved with mercuric chloride or zinc acetate, with exception of water samples collected for hydrogen and oxygen isotopic analysis. Pore waters were stored in cryogenic vials. Nontreated interstitial water aliquots were prepared for isotopic analysis of oxygen, hydrogen, DIC, carbon, boron, and strontium immediately after arrival in a shore-based laboratory.

Sedimentary pyrite was sampled for $\delta^{34}S$ analysis when collected in sufficient quantities. Sediments were collected from squeezed whole rounds for ICP-mass spectrometry (MS) analysis of major (Na, Mg, K, Ca, Ti, Mn, Fe, Al, Si, and P) and trace (Sr, Ba, Y, Zr, Co, Ni, Sc, and Rb) elements.

Organic geochemistry

Sediment hydrocarbon accumulations were quantified by headspace gas analysis (Pimmel and Claypool, 2001). A 5 cm^3 sediment headspace sample was collected every 10 m, heated, and the evolved gases were analyzed on gas chromatographs (GCs) dedicated to gas monitoring. Compositions of gases in sediment were determined at least once per core. Headspace gases were analyzed on either a Hewlett Packard 5890 Series II GC or a Hewlett-Packard 5890A natural gas analyzer (NGA). The first system determines concentrations of C_1 through C_3 hydrocarbons with a flame ionization detector (FID). A broader suite of hydrocarbon concentrations, ranging from C_1 to C_7, was detected with an FID and, concentrations of N_2, O_2, CO_2, Ar, and He were measured with a thermal conductivity detector (TCD) in the NGA. Chromatographic response on both GC instruments was calibrated against six different gas standards with variable quantities of low molecular weight hydrocarbons, N_2, O_2, CO_2, Ar, and He. Representative expansion void gases (EVGs) were collected directly through the core liner with an EVG sampler to prevent contact with ambient air. Gas concentrations were quantified, without the heating step, using the headspace GC method described above. Sediment samples were collected for land-based analysis of amino acid chirality, adenosine triphosphate (ATP), and acid and alkaline phosphatases (enzymatic activity).

Microbiology

Most subseafloor environments (deeper than 10 cm) are now recognized as very silent and low-activity biospheres based on recent advancements of subsurface microbiology (Whitman et al., 1998; D'Hondt et al., 2004; DeLong, 2004). However, the environments where energy sources for microbes are provided by geohydrological flow or sedimentation of organic matter are candidates for active or activated microbial processes. In the Gulf of Mexico, high sedimentation rates have been observed and strong geohydrological activity was expected. This situation suggests the possible presence of an active shallow subseafloor biosphere dependent on organic carbon as well as microbial communities in the deep subseafloor, activated by geohydrological flow.

Contamination testing

It is important to assess potential seawater contamination of sediments sampled for microbial analysis. Sediment microbial biomass decreases with depth and is in low abundance relative to the microbial biomass found in seawater. The fluorescent microparticle tracer method, as described in ODP *Technical Note* 28 (Smith et al., 2000), was applied during the expedition to quantify the extent of contamination produced during the coring process.

Latex fluorescent microspheres (Fluoresbrite carboxylate microspheres, 0.5 µm YG) were used as a particulate tracer. A 2 mL stock solution of microspheres was diluted with 40 mL of distilled water and sealed into a plastic bag. The bag was attached to the inside of the core catcher. The bag burst on impact into the sediments, and microspheres mixed with seawater and coated the core surface. During processing of whole-round cores, sediments from outer and inner layers were sampled by syringe for microscopic examination. The weighed samples were suspended in saturated NaCl solution to extract microspheres. The mixture was centrifuged at 1000 rpm for 5 min (Minispin, Eppendorf), and the supernatant was filtered onto black polycarbonate filters (Millipore; 0.2 µm). Fluorescent microsphere analysis was conducted with a Zeiss Axioplan fluorescence microscope equipped with the Zeiss number 9 filter set (BP 450–490; LP 520). The number of spheres observed was used to quantify contamination in spheres per gram of sample.

Core collection and sampling

In order to avoid contact with oxygen and monitor contamination, samples for microbiology were sampled immediately on the catwalk and brought into a glove box following subsampling for contamination testing. In the glove box, 2–3 cm^3 and 20–30 cm^3 of sediment were collected with a syringe for cultivation and tracer incubation analyses, respectively. Samples for cultivation

analysis were suspended in 20 mL of sterilized seawater, with and without Na_2S in glass vials, and sediment designated for tracer analysis was packed in anaerobic bags and stored at –80°C. The cultivation slurries were pressurized with nitrogen gas at 1.5 atm and stored at 5°C. An additional 1 cm^3 of sediment was extracted for microscopic observation (acridine orange direct counts [AODC] and fluorescence in situ hybridization [FISH], etc.) using a syringe. After these subsampling routines, the sediments for culture-independent molecular analyses based on deoxyribonucleic acid (DNA) (16S ribosomal ribonucleic acid [rRNA] gene clone analysis, quantitative polymerase chain reaction [PCR], etc.) were taken by spatula and stored in 50 mL plastic tubes at –80°C.

Microscopic observation (biomass count)

The sediments (1 cm^3) were sampled by syringe from whole-round core samples and suspended in 9 mL of sterilized seawater containing 3.7% neutralized formaldehyde. A 1 mL aliquot of the sediment suspension was stained with acridine orange. After staining for 1 h at 4°C, the sediment suspension was centrifuged for 5 s at 2000 × g and the supernatant was filtered through a 0.2 µm Isopore membrane filter (Millipore). The cells on the filters were counted under fluorescent light using a microscope. At least 50 microscopic fields for each sample were examined to determine the direct cell counts.

Physical properties

Shipboard measurements of physical properties quantify and contribute to characterizing variations in the sediment records caused by environmental changes, depositional and erosional events, and other geological phenomena. They further help to correlate core lithology, downhole geophysical logs, and seismic data.

Wet bulk density, compressional wave velocity, magnetic susceptibility, and electrical resistivity were measured on whole-core sections on the MST. Thermal conductivity measurements using the needle probe method were performed at discrete intervals in whole-round sections. Measurements made in undisturbed sections of split cores included compressional wave velocity in three directions, vane shear strength, and moisture and density (MAD) measurements, used to define bulk density, water content, grain density, dry bulk density, porosity, and void ratio. These laboratory methods were performed according to ODP laboratory practices (Blum, 1997). The undrained peak shear strength was also measured with a handheld penetrometer. Most measurements were performed at regularly spaced intervals, although some were taken in thin lithologic units that would have been missed by the regular sampling patterns. The flowchart of the analyses in the laboratory is shown in Figure **F8.**

Multisensor Track

The MST incorporates the gamma ray attenuation (GRA) densitometer, *P*-wave logger (PWL), magnetic susceptibility logger (MSL), and noncontact resistivity (NCR) detector. All MST measurements depend on core diameter and/or volume and therefore are most reliable in APC cores and undisturbed XCB cores. XCB cores often show drilling disturbance, have irregular variations in core diameter, and contain voids; corrections must be applied when these data are analyzed. At the drilling sites, drillover after APC refusal and XCB coring were used. All sections, excluding core catchers and those with deformed core liners, were run through the MST and the data were stored in the **Janus** database. Core sections were run through the MST after they had warmed to at least 17°C (measured at the top of the section).

All cores were processed through the MST before splitting. For Sites U1319 and U1320, NCR and magnetic susceptibility measurements were taken at 2 cm intervals. PWL and GRA measurements were taken at 4 cm intervals. At Site U1324 from Core 308-U1324B-5H and beyond and for all cores at Site U1322, all MST measurements were taken at 6 cm intervals because of the high core recovery rate.

Gamma ray attenuation bulk density

GRA bulk density is determined by comparing the attenuation of gamma rays through the cores with their attenuation through aluminum and distilled water standards. Recalibration was required approximately every 24 h. GRA bulk densities were calculated by means of shipboard software using calibration coefficients from the aluminum standard runs. Aluminum has a Compton mass attenuation coefficient of 0.10 cm^2/g, which is also valid for most common minerals. GRA bulk densities were not corrected for the presence of water, which has an attenuation coefficient of 0.11 cm^2/g. GRA bulk density provides a high-resolution data set used to fill trends between the MAD measurements and to compare with log-derived bulk density.

P-wave logger

The PWL transmits a 500 kHz compressional pulse wave through the core and core liner. Transmitting

and receiving transducers are aligned perpendicular to the long axis of the core. A pair of displacement transducers monitors the separation between the compressional wave transducers; variations in the outside diameter of the liner, therefore, do not degrade the accuracy of velocities. Water was sprayed on the outer surface of the core liner to enhance contact between transducers and liner. Poor contact between liner and sediment significantly degrades data.

Magnetic susceptibility logger

Magnetic susceptibility was measured on all sections using the 1.0 range on the Bartington Instruments magnetic susceptibility meter (model MS2) with an 80 mm diameter loop. Magnetic susceptibility, in addition to assisting with correlation between holes, aids in the detection of fine variations in magnetic intensity associated with magnetic reversals and lithologic changes. The quality of these results is degraded if the core liner is not completely filled and/or the core is disturbed. However, general downhole trends may still be used for core to well-log correlation.

Noncontact resistivity

The NCR technique operates by inducing a high-frequency magnetic field in the core from a transmitter coil, which induces electrical currents in the core that are inversely proportional to the resistivity. A receiver coil measures very small magnetic fields that are regenerated by the electrical current. To measure these very small magnetic fields accurately, a differential technique has been developed to compare the readings generated from the measuring coils with the readings from an identical set of coils operating in air. This technique provides the accuracy and stability required. The measurements are sensitive to core temperature and should be obtained in a stable temperature environment for best results. Calibration was achieved by filling short lengths (~25 cm each) of core liner with water containing known concentrations of NaCl. This provides a series of calibration samples with known resistivities that are then placed on the MST and logged. Resistivity is determined using the following equation;

$$r = Ax^B, \quad (1)$$

where

- r = resistivity (Ωm),
- A = calibration constant (0.1249),
- B = calibration constant (–0.7836), and
- x = resistivity output from the logger (mV).

NCR data are used for correlation with log-derived resistivity and as complementary data for interpretation of porosity and lithology.

Thermal conductivity

Thermal conductivity measurements on whole-round samples were made using the TK04 (Teka Bolin) system described by Blum (1997). Measurements were made once per core. Cores were allowed to equilibrate to ambient temperature before measurement. The measurement system employs a single needle probe (Von Herzen and Maxwell, 1959) heated continuously in full-space configuration. The needle probe contains a heater wire and a calibrated thermistor. At the beginning of each measurement, temperatures in the samples were monitored automatically, without applying a heater current, until the background thermal drift was <0.04°C/min. Once the samples were equilibrated, the heater circuit was closed and the temperature rise in the probe was recorded. The probe is assumed to be a perfect conductor because of its high conductance relative to the core sediments. Thus, during heating, temperature in the probe shows a linear relationship with the natural logarithm of time:

$$T(t) = (q/4\pi k)\ln(t) + C, \quad (2)$$

where

- T = temperature,
- q = heat input per unit length per unit time,
- k = thermal conductivity,
- t = time after heat initiation, and
- C = a constant.

Thermal conductivity (k) was determined using **Equation 2** by fitting the temperatures measured during the first 150 s of each heating experiment (see Kristiansen, 1982; Blum, 1997). The reported thermal conductivity value for each sample is the average of three repeated measurements. Data are reported in watts per meters degree Kelvin (W/[m·K]), with measurement errors of 5%–10% in high-quality cores. Corrections were not attempted for in situ temperature or pressure effects.

Compressional wave velocity

P-wave velocity measurements on split cores were carried out on the working-half core station along the x-, y-, and z-axis (Fig. **F9**). One measurement every two sections was performed. The locations for the *P*-wave measurements were generally next to the discrete MAD samples. When measuring PWS1, along the z-axis, and PWS2, along the y-axis, transducer pairs were inserted into the soft semiconsolidated sediment so that the measurement does not involve the core liner. PWS3 is designed to measure

the *P*-wave velocity along the x-axis through the core liner. The *P*-wave measurements were carried out in the order PWS3, PWS1, and PWS2 to minimize the disturbance by the transducer in the working half. When gas expansion prevented accurate measurements of *P*-wave velocity using PWS3; PWS2 and PWS1 were not used.

P-wave velocity is calculated by measuring the traveltime between transducers that are separated by a known distance. The distance is regularly measured with calipers and then assumed to be constant. The distance between the probe surfaces does not exactly correspond to the distance between the transducers. In addition, there is some electrical delay. The total delay was determined by inserting the probes into distilled water of known temperature and therefore of known acoustic velocity. This calibration was only performed after repeated use of the tool, which could have resulted in a change in distance between the probes. The temperature within the cores was measured for correction of the measured *P*-wave velocity. The presented data are uncorrected for in situ temperature and pressure. These corrections can be made using the relationships outlined in Wyllie et al. (1956), Wilson (1960), and Mackenzie (1981). For measurements with the PWS3 contact probe, the instrument is equipped with a digital scale unit that allows precise determination of sample thickness. A Tectronix signal generator, differential amplifier, and oscilloscope are used to transmit and receive signals from all three transducer pairs and to digitize analog waveform data.

The anisotropy of *P*-wave velocity (or acoustic anisotropy, measured in percent) is defined here, following Carlson and Christensen (1977), as the difference between velocities in the horizontal and vertical directions expressed as a percentage of the mean velocity:

$$\text{Anisotropy} = [(v_{pl} - v_{pt})/0.5(v_{pl} + v_{pt})] \times 100, \quad (3)$$

where

- v_{pl} = *P*-wave velocity measured in the direction parallel (longitudinal or z-axis) to the core axis and
- v_{pt} = *P*-wave velocity in the horizontal (transverse, x- or y-axis) direction.

In clay-rich marine sediments, positive transverse anisotropy will vary from 0% near the surface (isotropic) to >12% at depths of several hundred meters (Brückman et al., 1997). Sources for *P*-wave anisotropy include (but are not limited to) (1) compactional anisotropy (preferential alignment of pores and particles parallel to bedding because of gravitational compaction under increasing overburden) and (2) presence of microstructures such as microfractures and microcracks.

Moisture and density

MAD parameters including bulk density, grain density, and porosity were determined from wet mass, dry mass, and dry volume measurements of split core sediments after method C of Blum (1997). For each core section, at least one sample of ~10 cm^3 was taken and placed in a 10 mL glass beaker. Care was taken to sample undisturbed parts of the core and to avoid sampling drilling fluid. The wet weight of the samples was measured, and then the samples were dried for at least 24 h in an oven at 105°C. The samples cooled in a desiccator to room temperature. Dry weight was measured, after which volume was determined using a pycnometer.

Sample mass was determined to a precision of 0.01 g using two Scientech 202 electronic balances and a computer averaging system to compensate for ship motion. The reference mass was always set to be within a 5 g margin of the actual sample weight. Sample volumes were determined using two helium-displacement penta-pycnometers with a precision of 0.02 cm^3. Volume measurements were repeated three times, until the last two measurements exhibited <0.1% standard deviation. A reference volume was used to calibrate the pycnometers and to check for instrument drift and systematic error.

Moisture content, grain density, bulk density, and porosity were calculated from the measured wet mass, dry mass, and dry volume as described by Blum (1997). The presented data are corrected for the mass and volume of evaporated seawater assuming a seawater salinity of 35 ppt. This results in a fluid density of 1.024 g/cm^3 assuming a salt density of 2.20 g/cm^3.

Shear strength

Undrained shear strength was measured using the automatic vane shear (AVS) and a pocket penetrometer. The measurements were not performed at in situ stress conditions and thereby underestimate the true undrained peak shear strength in situ. All shear strength measurements were performed in the y–z plane (see Fig. **F9**).

Automatic vane shear system

Undrained shear strength (τ_{fu}) was measured in fine-grained, plastic sediment using the AVS system following the procedures of Boyce (1977). The vane rotation rate was set to 90°/min. Measurements were

made only in fine-grained sediment. Peak undrained shear strength was measured typically at every second section. The instrument measures the torque and strain at the vane shaft using a torque transducer and potentiometer. The peak shear strength was determined from the torque versus strain plot. The experiment was set up to run for 6 min, which equals 1.5 vane laps. The residual shear strength was taken to be the lowest measured shear strength after reaching the peak value during the test cycle. All shear strengths were measured with the rotation axis parallel to the bedding plane.

Penetrometer

A pocket penetrometer (Geotester STCL-5) was used to obtain additional undrained shear strength measurements. The penetrometer is a flat-footed, cylindrical probe that is pushed 6.4 mm into the split-core surface. The penetrometer is calibrated as an unconfined compression test, which (for an ideal clay) measures twice the undrained shear strength, or $2\tau_{fu}$ (Holtz and Kovacs, 1981). The scale on the dial is converted into shear strength (in kilopascals) using the following equation:

$$\tau_{fu} = [(S_u \times 10) \times g]/2, \quad (4)$$

where

- τ_{fu} = undrained shear strength (kPa),
- S_u = penetrometer reading (kg/cm^2), and
- g = acceleration due to gravity (9.81 m/s^2).

The maximum shear strength that can be measured with the pocket penetrometer is 220 kPa. Penetrometers are designed for use in soft sediment, and readings were discarded if the sediment cracked during measurement. Measurements using the penetrometer were typically performed every second section.

Presentation of undrained shear strength

For every site, the undrained shear strength is presented in plots with the undrained peak and the residual shear strength from the AVS system, a comparsion between the undrained peak shear strength measured by the AVS system and the penetrometer, the sensitivity, and a plot of the undrained peak strength versus the hydrostatic vertical effective stress.

The peak undrained shear strength measured with the AVS system is defined as the peak value during the shearing procedure, and the residual undrained shear strength is defined as the lowest measured undrained shear strength during the shearing period (1.5 laps). If a negative value was achieved during the test, the residual shear strength was set to 0 kPa. The penetrometer only measured the undrained peak shear strength.

Sensitivity (S_n) is here defined as the ratio between the peak and residual undrained shear strength from the AVS system.

$$S_n = \frac{\tau_{fu}^{peak}}{\tau_{fu}^{res}}. \quad (5)$$

Sensitivity allows estimation of the loss in strength of a sediment sample when the undrained shear stress exceeds the corresponding undrained peak shear strength.

The total vertical stress (σ_v) and vertical hydrostatic effective stress (σ_{vh}') are estimated using bulk density data and hydrostatic stress conditions (Equations 6 and 7);

$$\sigma_v = \int_0^z \rho(z) g dz \quad \text{and} \quad (6)$$

$$\sigma_{vh'} = \int_0^z (\rho(z) - \rho_w) g dz, \quad (7)$$

where

- z = depth beneath the seafloor,
- $\rho(z)$ = bulk density at depth z,
- g = acceleration due to gravity (9.81 m/s^2), and
- ρ_w = the pore fluid density, which is assumed to be 1.024 g/cm^3 (seawater) (= 1024 kg/m^3).

Downhole measurements

In situ temperature and pressure measurements

Several downhole tools were deployed during Expedition 308 to measure in situ temperature, formation pressure, and hydraulic conductivity. Temperature and pressure data are critical for constraining sediment properties and flow fields. In addition, temperature affects sediment diagenesis and microbial activity.

Temperature, pressure, and hydraulic conductivity were measured in situ with a newly developed temperature/dual pressure (T2P) probe and the Davis-Villinger Temperature-Pressure Probe (DVTPP). In situ temperature measurements were also made using the APC temperature (APCT) tool.

Temperature/dual pressure probe

A narrow-diameter penetration probe with one temperature and two pressure sensors (T2P) was deployed during Expedition 308 to evaluate in situ fluid pressure, hydraulic conductivity, and temperature in low-permeability sediments. The T2P mea-

sures pressure and temperature at the tool tip and pressure 21 cm up-probe from the tip measurement (Fig. F10). The needle probe diameter is 0.6 cm at the tip and 3.6 cm at the upper pressure port. A 3.6 cm diameter drive tube extends 100 cm above the shaft pressure sensor where the drive tube connects with the data acquisition unit. All deployment data are stored in memory in the data acquisition unit.

The T2P interfaces with the colleted delivery system (CDS) used to deploy other downhole tools such as the DVTPP. The CDS is lowered by wireline and engages in the bottom-hole assembly (BHA). Once the CDS is engaged in the BHA, the drill string is used to push the needle shaft and drive the tube into the formation. This penetration causes pressure and temperature increases. After penetration into the formation, the drill string is raised 3–4 m uphole and the CDS telescopes. The telescope action leaves the T2P in the formation and effectively decouples the probe from the drill string. The T2P remains in the formation to measure pressure and temperature. Dissipation of pressure and temperature is used to determine in situ pressure, hydraulic conductivity, and temperature. After adequate time for dissipation (30–90 min), the wireline pulls the CDS to its extended position and then pulls the T2P out of the formation. The CDS and T2P are pulled to the surface, where the data are downloaded from the data acquisition unit.

The slim design of the T2P facilitates rapid, high-quality measurement of in situ conditions in low-permeability sediment. The design minimizes pressure and temperature pulses generated during penetration. The two pressure sensors have different dissipation rates because they are at different diameters on the tool. Comparison of the dissipation curves allows equilibrium pressure to be interpreted with less recorded dissipation than if one sensor was used.

Davis-Villinger Temperature-Pressure Probe

The DVTPP is a modified version of the Davis-Villinger Temperature Probe (DVTP) (see Davis et al., 1997; Pribnow et al., 2000; Graber et al., 2002). The DVTPP provides simultaneous measurement of formation temperature and pressure. The probe tip incorporates a single thermistor in an oil-filled needle and ports that allow hydraulic transmission of formation pressure to an internal Paroscientific pressure gauge. A standard data logger records the pressure and temperature data. Thermistor sensitivity is 0.02 K in an operating range of –5° to 20°C.

A typical DVTPP deployment consists of connecting the DVTPP to the CDS and lowering the tool string by wireline to the seafloor and then holding for 10 min. The drill bit is then raised 12 m off the bottom of the hole. Subsequently, the tool string is lowered until the CDS engages in the BHA, with the tip of the tool extending 1.1 m below the drill bit. The DVTPP is pushed into the sediment by lowering the drill bit, the CDS is telescoped to decouple the DVTPP and the drill string, and pressure is recorded for ~40 min. The tool string is then recovered via wireline. All data are stored in memory. If smooth pressure decay curves are recorded after penetration then theoretical extrapolations to in situ pore pressure are possible. Decay time is a function of the sediment permeability and the magnitude of the initial insertion pressure, which is a function of the taper angle and diameter of the tool (Whittle et al., 2001; Heeseman, 2002). Temperature decay of the frictional heat generated during insertion of the DVTPP can be used to interpret the formation temperature. Temperature decays faster than pressure.

Advanced Piston Corer Temperature tool

The APCT tool fits into the cutting shoe on the APC and is used to measure sediment temperatures during regular APC coring. The tool contains electronic components, including battery packs, a data logger, and a platinum resistance-temperature device that is calibrated from 0° to 30°C. Descriptions of the tool and of the principles behind data analysis can be found in Pribnow et al. (2000) and Graber et al. (2002). The thermal time constant of the cutting shoe assembly where the APCT tool is inserted is ~2–3 min. The only modification to normal APC procedures required to obtain temperature measurements is to hold the corer in place for ~10 min after cutting the core. During this time, the APCT tool logs temperature on an internal microprocessor. Following deployment, the data are downloaded for processing. The tool can be preprogrammed to record temperatures at a range of sampling rates. A sampling rate of 10 s was used during Expedition 308. A typical APCT measurement consists of a seafloor temperature record lasting 10 min for the first deployment in each borehole and 2 min during subsequent deployments. This is followed by frictional heating pulse when the piston is fired, and the resultant temperature decay is monitored for 10 min. A final frictional pulse is generated upon removal of the corer from the sediment.

Downhole logging

The downhole logging program during Expedition 308 was designed to

- Assess how pressure, stress, and geology control fluid migration on a passive margin;
- Establish reference geotechnical and petrophysical properties at a location where overpressure is not present as well when overpressure is present;

- Learn about factors controlling slope (in)stability;
- Determine major depositional events and timing of landslides; and
- Provide information about turbidite processes along the continental slope.

In addition, the downhole measurements plan was established to define structural and lithologic boundaries, establish site-to-site correlations, provide ties to seismic data, produce direct correlations with laboratory data, and identify conduits that may serve as pathways for fluid migration. Finally, downhole measurements complemented core measurements by filling gaps in stratigraphy, determined lithogical interpretations in intervals of poor core recovery, and provided the means for correlation with the seismic data.

Logging while drilling and measurement while drilling

During Expedition 308, four Schlumberger logging-while-drilling (LWD) and measurement-while-drilling (MWD) tools were deployed at each site in the Brazos-Trinity and Ursa Basins. LWD surveys have been successfully conducted during ODP Legs 156 (Shipley, Ogawa, Blum, et al., 1995), 170 (Kimura, Silver, Blum, et al., 1997), 171A (Moore, Klaus, et al., 1998), 174A (Austin, Christie-Blick, Malone, et al., 1998), 188 (O'Brien, Cooper, Richter, et al., 2001), 193 (Binns, Barriga, Miller, et al., 2002), 196 (Mikada, Becker, Moore, Klaus, et al., 2002), 204 (Tréhu, Bohrmann, Rack, Torres, et al., 2003), and 209 (Kelemen, Kikawa, Miller, et al., 2004).

LWD and MWD tools measure different parameters. LWD tools measure formation properties with instruments located in the drill collars above the drill bit. MWD tools are also located in the drill collars and measure downhole drilling parameters (e.g., weight on bit, torque, etc.). The difference between LWD and MWD tools is that LWD data are recorded in memory and retrieved when the tools reach the surface, whereas MWD data are transmitted through the drilling fluid within the drill pipe by means of a modulated pressure wave, or mud pulsing, and monitored in real time. MWD tools enable both LWD and MWD data to be transmitted uphole when the tools are used in conjunction. LWD is often used generically for LWD and MWD measurements.

LWD and MWD tools used during Expedition 308 included the GeoVision Resistivity (GVR) tool, PowerPulse MWD tool, Array Resistivity Compensated (ARC) tool, and Vision Density Neutron (VDN) tool. This was the first time the ARC tool was used within ODP/IODP. Figure **F11** shows the configuration of the LWD/MWD BHA, and Table **T1** lists the set of measurements recorded.

LWD provides measurements before the sediments experience the adverse effects of continued drilling or coring operations. Fluid invasion into the borehole wall is reduced relative to wireline logging because of the shorter elapsed time between drilling and logging.

The LWD tools are battery powered and use erasable/programmable read-only memory chips to store data until they are downloaded. The LWD tools take measurements at evenly spaced time intervals and are synchronized with a system on the drilling rig that monitors time and drilling depth. LWD data are downloaded from each tool through an RS-232 serial link to a laptop computer. Synchronization of the uphole and downhole clocks allows merging of the time-depth data (from the surface system) and the downhole time-measurement data (from the tools). The resulting depth-measurement data are transferred in the downhole measurements laboratory (DHML) on board the *JOIDES Resolution* for reduction and interpretation.

Depth-tracking systems

LWD tools record data versus time. The Schlumberger Integrated Drilling and Logging (IDEAL) system records the time and depth of the drill string below the rig floor. As shown in Figure **F12**, LWD operations aboard the *JOIDES Resolution* require accurate and precise depth tracking and the ability to independently measure and evaluate the movement of (1) the position of the traveling block in the derrick, (2) the heave of the vessel by the action of waves/swells and tides, and (3) the action of the motion compensator.

Motion compensator and drawworks encoders

The length of the drill string (combined lengths of the BHA and the drill pipe) and the position of the top drive in the derrick are used to determine the depth of the drill bit and rate of penetration. The system configuration is illustrated in Figure **F12** and is further described below.

Drilling line is spooled on the drawworks. From the drawworks, the drilling line extends to the crown blocks, which are located at the top of the derrick, and then down to the traveling block. The drilling line is passed several times, usually six or eight times, between the traveling blocks and the crown blocks and then fastened to a fixed point called the deadman anchor. The driller controls the drawworks, which, via the pulley system, control the position of the traveling block in the derrick.

Aboard the *JOIDES Resolution*, the heave motion compensator is suspended from the traveling block. The top drive is attached to the motion compensator. The motion compensator uses pressure-charged pistons to provide a buffer against waves and swell. As the vessel rises, the pressure on the pistons increases and they extend to keep the bit on bottom, whereas when the vessel drops, the pistons retract and diffuse any extra weight from being stacked on the bit.

The drill string is connected to the top drive; therefore, movement of the top drive needs to be measured to provide the drill string depth.

To measure the movement of the traveling blocks, a drawworks encoder (DWE) is mounted on the shaft of the drawworks. One revolution of the drawworks will pay out a certain amount of drilling line and, in turn, move the traveling blocks a certain distance. Calibration of the movement of the traveling block to the revolutions of the drawworks is required.

Hookload sensor

A hookload sensor measures the weight of the load on the drill string and can detect whether the drill string is disconnected from the traveling block and held fast at the rig floor ("in-slips"). When drilling ahead, the string is "out-of-slips." When the drill string is in-slips, motion from the blocks or motion compensator will not have any effect on the depth of the bit (i.e., it will remain stationary) and the DWE information does not augment the recorded bit depth. When the drill string is out-of-slips, the DWE information augments the recorded bit depth. The difference in hookload weight between in-slips and out-of-slips is distinguishable. The heave of the ship will continue to affect the bit depth whether the drill string is in-slips or out-of-slips.

Heave motion sensors

On the *JOIDES Resolution*, vessel heave is measured in two ways. The rig instrumentation system measures and records the heave of the ship and the motion of the cylinder of the active compensator on the rig floor. The motion compensator cylinder extends and retracts to compensate for ship heave, which is detected by fixed accelerometers. Heave and cylinder position are transmitted to the Schlumberger recording system via the Wellsite Information Transfer System (WITS) line. Software filtering may be used to smooth the time-depth file by applying a weighted average to the time-depth data based on the observed amplitude and period of ship heave. Depth-filtering has improved the quality of GVR image logs from previous ODP holes.

GeoVision Resistivity tool

The GVR tool provides formation resistivity and electrical images of the borehole wall, similar to the Formation MicroScanner (FMS), but with complete coverage of the borehole walls and lower vertical and horizontal resolution. In addition, the GVR tool contains a scintillation counter that provides a total gamma ray measurement (Fig. **F13**). Because a caliper log is not available without other LWD measurements, the influence of the shape of the borehole on the log responses cannot be directly estimated.

The GVR tool is connected directly above the drill bit and uses the lower portion of the tool and the bit as a measuring electrode. This provides a bit resistivity measurement with a vertical resolution just a few centimeters longer than the length of the bit. A 2.5 cm electrode located 91 cm from the bottom of the tool provides a focused lateral resistivity measurement (RES_RING) with a vertical resolution of 5 cm. The characteristics of RES_RING are independent of where the GVR tool is placed in the BHA; its depth of investigation is ~18 cm. Button electrodes provide shallow-, medium-, and deep-focused resistivity measurements and azimuthally oriented images. These images reveal information about structure and lithologic contacts. The button electrodes are ~2.5 cm in diameter and reside on a clamp-on sleeve. The buttons are longitudinally spaced along the GVR tool to render staggered depths of investigation of ~2.5, 7.6, and 12.7 cm. The tool's orientation system uses Earth's magnetic field as a reference to determine tool position with respect to the borehole as the drill string rotates, thus allowing azimuthal resistivity and gamma ray measurements. Measurements are acquired with a ~6° azimuthal resolution. The vertical resolution for each resistivity measurement is shown in Figure **F13.**

The diameter of the GVR measuring button sleeve is 23.3 cm, and the diameter of the three-cone rotary bit used during Expedition 308 is 25 cm. This results in a 1.7 cm gap, or "standoff," between the resistivity buttons and the formation. The standoff causes the formation resistivity to be underestimated slightly, depending on the ratio between the formation and borehole fluid resistivity. For a resistivity ratio <100, as expected for Expedition 308 sites, a resistivity correction factor of as much as 4% may be applied to each GVR measurement. Estimated correction factors for the GVR tool are given in Table **T2** (Schlumberger, unpubl. data [2001]). Because of its limited depth of penetration into the formation, the correction factor for shallow button resistivity cannot be constrained.

GVR programming

All data are collected at a minimum vertical density of 15 cm whenever possible; hence, a balance must

be determined between rate of penetration (ROP) and sampling rate. This relationship depends on the recording rate, the number of data channels to record, and the memory capacity (46 MB) of the LWD tool. During Expedition 308, we used sampling rate of 5 s for high-resolution GVR images. The maximum ROP allowed to produce 1 sample/15 cm interval is given as follows:

$$\text{ROP (m/h)} = 548/\text{sample rate}. \quad (8)$$

This relationship gives 110 m/h maximum ROP for the GVR and 18 m/h minimum. For Expedition 308, the target ROP was 25 m/h, ~23% of the maximum ROP. This rate improves the vertical resolution of the resistivity images to 5–10 cm per rotation. Under this configuration, the GVR tool has enough memory to record 150 h of data. This was sufficient to complete the scheduled LWD operations at the Expedition 308 drill sites.

Bit resistivity measurements

For the bit resistivity measurements, a lower transmitter (T2) produced a current and a monitoring electrode (M0) located directly below the ring electrode measured the current returning to the collar (Fig. **F13**). When connected directly to the bit, the GVR tool used the lower few inches of the tool as well as the bit as a measurement electrode. The bit resistivity measurement (RES_BIT) had a depth of investigation of 81 cm.

Ring resistivity measurements

The upper and lower transmitters (T1 and T2, respectively) produce currents in the collar that meet at the ring electrode. The sum of these currents is focused radially into the formation. These current patterns can become distorted depending on the strength of the fields produced by the transmitters and the formation around the collar. Therefore, the GVR tool uses a cylindrical focusing technique that takes measurements in the central (M0) and lower (M2) monitor coils to reduce distortion and create an improved ring response. The ring electrode is held at the same potential as the collar to prevent interference with the current pattern. The current required for maintaining the ring at the required potential is measured and related to the resistivity of the formation. The narrow ring electrode (~4 cm) provides a resistivity measurement (RES_RING) with 5 cm vertical resolution.

Button resistivity measurements

The button electrodes function the same way as the ring electrode. Each button is electrically isolated from the body of the collar but is maintained at the same potential to avoid interference with the current field. The amount of current required to maintain the button at the same potential is related to the resistivity of the formation. The buttons are 4 cm in diameter, and the shallow-, medium-, and deep-resistivity measurements (RES_BS, RES_BM, and RES_BD, respectively) can be acquired azimuthally as the tool rotates within 56 sectors to produce a borehole image.

Array resistivity compensated tool

The ARC tool is capable of multidepth borehole-compensated real-time and memory resistivity and gamma ray measurements at 2 MHz and 400 kHz (Fig. **F14**). The measured resistivity utilizes electromagnetic wave propagation in the formation. It has five transmitters and two receivers, giving five phase and five attenuation resistivities for each frequency. Each measurement is compensated for borehole rugosity using mixed borehole compensation. It also contains a plateau gamma ray detector for correlation. The gamma ray measurement point for the ARC tool is 7.6 cm behind the resistivity measurement point. Also included in the collar is the annular pressure-while-drilling (APWD) sensor, located 69 cm ahead of the resistivity measure point. The APWD sensor measures borehole annulus pressure and temperature.

Measurement-While-Drilling (PowerPulse) tool

The Schlumberger MWD PowerPulse tool (Fig. **F15**) was deployed in combination with LWD tools. The MWD tool had previously been deployed during ODP Legs 188 (O'Brien, Cooper, Richter, et al., 2001), 196 (Mikada, Becker, Moore, Klaus, et al., 2002), and 204 (Tréhu, Bohrmann, Rack, Torres, et al., 2003). MWD tools measure downhole drilling parameters, immediately above the ARC tool (Fig. **F11**).

MWD data are transmitted by means of a pressure wave (mud pulsing) through the fluid within the drill pipe. The 17.15 cm diameter MWD PowerPulse tool generates a continuous mud-wave transmission within the drilling fluid and changes the phase of this signal (frequency modulation) to transmit relevant bits representing the sensor data (Fig. **F16**). Pressure sensors attached to a standpipe on the rig floor and on the gooseneck on the crown block measure the pressure wave pulsed by the MWD tool. Pulse rates of 12 bps were achieved during Expedition 308.

Parameters transmitted by mud pulses included downhole weight on bit (DWOB), downhole torque on bit (DTOR), torsional vibration, lateral shock, and tool stick-slip (Table **T1**). Measurements are made us-

ing paired strain gauges, accelerometers, and lateral shock near the base of the MWD collar. Comparison of MWD drilling parameter data, rig instrumentation system data, and ship-heave information was used to improve drilling control and to assess the quality of the recorded LWD data.

The mud pulse system also transmitted annular pressure, temperature, equivalent circulating density, gamma radiation, resistivity, density, and porosity from the LWD tools. Measurement parameters from each LWD collar were updated at rates corresponding to 15 cm to 1.5 m depth intervals, depending on the initialized values and ROP of the tool. These data confirmed the operational status of each tool and provided real-time logs for identifying lithologic contacts and potential shallow-water flow or overpressured zones.

Vision Density Neutron tool

The density section of the VDN tool uses a 1.7 Ci (Curie = 3.7×10^{10} Bq), ^{137}Cs gamma ray source in conjunction with two gain-stabilized scintillation detectors to provide borehole-compensated density. The detectors are located 12.7 and 30.48 cm below the source (Fig. **F17**). The number of Compton scattering collisions (change in gamma ray energy by interaction with the formation electrons) is related to formation density. Returns of low-energy gamma rays are converted to a photoelectric effect (PEF) value, measured in barns per electron. PEF depends on electron density and hence responds to bulk density and lithology (Anadrill-Schlumberger, 1993). It is particularly sensitive to low-density and high-porosity zones.

The gamma ray source and detectors are positioned behind holes in the fin of a full-gauge 24.5 cm diameter clamp-on stabilizer (Fig. **F17**). This geometry forces the sensors against the borehole wall to reduce the effects of borehole irregularities. The vertical resolution of the density and PEF measurements is ~15 and 5 cm, respectively. For measurement of tool standoff, a 670 kHz ultrasonic caliper is available on the VDN tool. The ultrasonic sensor is aligned with and located just below the density detectors. The sensor can also be used as a quality control check for the density measurements. Neutron porosity measurements are obtained using fast neutrons emitted from a 10 Ci americium oxide–beryllium (AmBe) source. Hydrogen quantities in the formation largely control the rate at which the neutrons slow down to epithermal and thermal energies. The energy of the detected neutrons has an epithermal component because much of the incoming thermal neutron flux is absorbed as it passes through the 2.54 cm drill collar. Neutrons are detected in near- and far-spacing detector banks, located 30.48 and 60.96 cm above the source. The vertical resolution of the tool under optimum conditions is ~34 cm. The neutron logs are affected by the different lithologies because the tool is calibrated for 100% limestone. Neutron porosity logs are processed to eliminate the effects of borehole diameter, tool size, temperature, drilling mud hydrogen index (dependent on mud weight, pressure, and temperature), and mud. Formation fluid salinity, lithology, and other environmental factors also affect neutron porosity. These parameters must be estimated for each borehole during neutron log processing (Schlumberger, 1994).

Data output from the VDN tool includes apparent neutron porosity (i.e., the tool does not distinguish between pore water and lattice-bound water), formation bulk density, and PEF. Because of the lack of quadrant data, density logs have been "rotationally processed" to show the image-derived density (IDRO). The IDRO algorithm uses the bulk density image from the VDN tool to compute a single density. It identifies which sectors at each depth level provide the highest-quality density measurements and computes a density based on those sectors while the tool is rotating. The VDN tool also outputs a density caliper record based on the standard deviation of density measurements made at high sampling rates around the circumference of the borehole. The measured standard deviation is compared with that of an in-gauge borehole, and the difference is converted to the amount of borehole enlargement (Anadrill-Schlumberger, 1993). A standoff of <2.54 cm between the tool and the borehole wall indicates good borehole conditions, for which the density log values are considered to be accurate to ±0.015 g/cm^3 (Anadrill-Schlumberger, 1993).

LWD/MWD data flow

MWD data were monitored in the onboard downhole measurements laboratory (DHML) and displayed in the drillers shack, operations superintendent's office, co-chiefs' office, and core laboratory.

The main parameters monitored were the equivalent circulating density relative to seafloor (ECD_{rsf}), annular pressure while drilling (APWD), annular pressure while drilling above hydrostatic (APWD*), resistivity measurements from the GVR, gamma ray measurements from the GVR, and the density caliper (DCAV). ECD_{rsf} was calculated as follows:

$$ECD_{rsf} = (P_{apwd} - P_{wsf})/[(D_{apwd} - D_w - RKB) \times 0.0519], \quad (9)$$

where

ECD_{rsf} = equivalent circulating density relative to seafloor (lb/gal [ppg]);
P_{apwd} = APWD reading (lb/in^2 [psi]);

P_{wsf} = water pressure at seafloor (lb/in² [psi]);
D_{apwd} = TVD (true vertical depth) of APWD sensor (ft);
D_w = water depth (ft);
RKB = distance from sea level to dual elevator stool (ft); and
0.0519 = conversion factor.

Hydrostatic pressure at the seafloor is

$$P_{wsf} = ECD_{sw} \times D_w \times 0.0519, \quad (10)$$

where ECD_{sw} = equivalent mud weight of seawater (8.65 lb/gal [ppg]).

Wireline logging tools

Wireline logs reveal the physical, chemical, and structural properties of formations. Where core recovery is good, core data are used to calibrate the geophysical signature of the rocks. In intervals of low core recovery or disturbed cores, log data may provide the only way to characterize sediments. Wireline logs also aid in linking core data and seismic reflection data. Individual logging tools are joined together into tool strings (Fig. **F18**); consequently, several measurements can be made during one logging run (Table **T3**). The tool strings are lowered to the bottom of the borehole on a wireline, and data are logged as the tool string is pulled back up the borehole. Repeat runs improve coverage and confirm the reproducibility of logging data.

Wireline logging tool strings

Three logging strings were deployed during Expedition 308 (Fig. **F18;** Table **T3**):

- The triple combination (triple combo) tool string consisting of the Hostile Environment Gamma Ray Sonde (HNGS), Phasor Dual Induction–Spherically Focused Resistivity (DIT-SFR) tool, Hostile Environment Litho-Density Tool (HLDT), and Accelerator Porosity Sonde (APS). The Lamont-Doherty Earth Observatory (LDEO) high-resolution Temperature/Acceleration/Pressure (TAP) tool was attached at the bottom of this tool string, and the Inline Check Shot Tool (QSST) was added at the top.
- The FMS-sonic tool string consisting of the FMS, General Purpose Inclinometer Tool (GPIT), Scintillation Gamma Ray Tool (SGT), and Dipole Sonic Imager (DSI).
- The Well Seismic Tool (WST).

Tool acronyms, parameters measured sample intervals, and vertical resolution are summarized in Tables **T3** and **T4.**

Wireline logging data flow and processing

Data for each wireline logging run were recorded and stored digitally and monitored in real time using the Schlumberger MAXIS 500 system. After logging was completed in each hole, data were transferred to the shipboard DHML for preliminary processing and interpretation. FMS image data were interpreted using the Schlumberger GeoFrame (version 4.0.42) software package. Well seismic, sonic, and density data were used for calculation of synthetic seismograms to establish the seismic-to-borehole tie.

Logging data were also transmitted to LDEO Borehole Research Group (BRG) using a satellite high-speed data link for processing. Data processing at LDEO-BRG consisted of (1) depth-shifting all logs relative to a common datum (i.e., mbsf), (2) corrections specific to individual tools, and (3) quality control. Processed data were transmitted back to the ship. Further postcruise processing of the logging data from the FMS was performed at LDEO-BRG. Postcruise-processed data in ASCII are available from **iodp.ldeo.columbia.edu/DATA/index.html.** At the end of each expedition, a summary of "logging highlights" is posted on the USIO JOI Alliance Web site (**iodp.ldeo.columbia.edu/LOG_SUM/index.html**).

Wireline log data quality

Log data quality may be degraded where borehole diameter greatly decreases or is washed out. Deep-investigation measurements such as resistivity and sonic velocity are least sensitive to borehole conditions. Nuclear measurements (density and neutron porosity) are more sensitive because of their shallow depth of investigation and the effect of drilling fluid volume on neutron and gamma ray attenuation. Corrections can be applied to the original data to reduce these effects. The effects of very large washouts, however, cannot be corrected. HNGS and NGT data provide a depth correlation between logging runs. Logs from different tool strings may have minor depth mismatches caused by either cable stretch or ship heave during recording.

Interpreting structure from GVR and FMS images

Structural data were determined from unwrapped 360° GVR images using the Schlumberger GeoFrame software. The image orientation is referenced to north, as measured by the magnetometers inside the tool, and the hole is assumed to be vertical. Horizontal features appear horizontal on the images, whereas planar dipping features are sinusoidal in unwrapped images. Sinusoids are interactively fitted to beds and fractures to determine dip and azimuth, and the data are exported from GeoFrame for further analysis.

Resolution for GVR images is 5–10 cm, compared to millimeters within cores and 0.5 cm for FMS images. This should be considered when directly comparing reports. The GVR tool provides 360° coverage; whereas the FMS provides higher-resolution data, but coverage is restricted to ~30% of the borehole. Fractures were identified within GVR images by their anomalous resistivity or conductivity and from contrasting dip relative to surrounding bedding trends. Differentiating between fractures and bedding planes can be problematic, particularly if both are steeply dipping with similar orientations.

During processing, quality control of the data is mainly performed by cross-correlation of all logging data. Large (>30 cm) and/or irregular borehole diameter affects most recordings, particularly the HLDS, which requires centralization and good contact with the borehole wall. Hole deviation can also negatively affect the data; the FMS, for example, is not designed to be run in holes with >10° deviation, as the tool weight might cause the caliper to close.

FMS image processing is required to convert the electrical current in the formation into an image representative of the conductivity. This is achieved through two processing phases: data restoration and image display. During the data restoration process, speed corrections, image equalization, button correction, emitter exciter (EMEX) voltage correction, and depth-shifting techniques are applied.

Speed corrections use the data from the z-axis accelerometer to correct the vertical position of the data for variations in the speed of the tool (i.e., GPIT speed correction), including tool sticking and slipping. In addition, an image-based speed correction is also applied to the data. This correction checks the GPIT speed correction.

Image equalization is the process whereby the average response of all the buttons is normalized over large intervals to correct for various tool and borehole effects. These effects include differences in the gain and offset of the preamplification circuits associated with each button and differences in contact with the borehole wall between buttons on a pad and between pads. If the measurements from a particular button are unreasonably different from adjacent buttons (e.g., "dead buttons") over a particular interval, they are declared faulty and the defective trace is replaced by traces from adjacent good buttons. The button current response is controlled by the EMEX voltage, which is applied between the button electrode and the return electrode. The EMEX voltage is regulated to keep the current response within the operating range. The button response is divided by the EMEX voltage, and, as a result, the response corresponds more closely to the conductivity of the formation.

Each of the logging runs are depth-matched to a common scale by means of lining up distinctive features of the natural gamma log from each of the tool strings. If the reference-logging run is not the FMS-sonic tool string, the specified depth shifts are applied to the FMS images. The position of data located between picks is computed by linear interpolation.

Once the data are processed, both static and dynamic images are generated. In static normalization, a histogram equalization technique is used to obtain the maximum quality image. In this technique, the resistivity range of the entire interval of good data is computed and partitioned into 256 color levels. This type of normalization is best suited for large-scale resistivity variations. The image can be enhanced when it is desirable to highlight features in sections of the borehole where resistivity contrasts are relatively low when compared with the overall resistivity range in the section. This enhancement is called dynamic normalization. By rescaling the intensity over a smaller interval, the contrast between adjacent resistivity levels is enhanced. With dynamic normalization, resistivities in two distant sections of the hole cannot be directly compared. The interval used for the dynamic normalization was 2 m.

FMS images are displayed as an unwrapped borehole cylinder with a circumference derived from the bit size. Several passes can be oriented and merged together on the same presentation to give additional borehole coverage where the tool pads followed a different track during the second logging pass. A dipping plane in the borehole can be displayed as a sinusoid on the image, and the amplitude of this sinusoid is proportional to the dip of the plane. The images are oriented with respect to north.

Core-log-seismic correlation

We correlated core physical properties, wireline logs, LWD logs, and two-dimensional (2-D) and three-dimensional (3-D) seismic survey data in the Brazos-Trinity IV and Ursa Basins. To ensure accurate correlation of the data, it was important to ascertain the accuracy of the navigation of each survey, the hole deviation, the drill string position at the seafloor relative to the sea surface, the accuracy of the depth-converted seismic data, and the vertical and horizontal seismic resolution. Accurate correlation is critical to extend the study of the direct measurements of the subsurface physical properties away from the borehole using the seismic data. In order to correlate the 2-D/3-D seismic data with the LWD data, synthetic seismograms were constructed using densities and velocities for each site.

References

Anadrill-Schlumberger, 1993. *Logging While Drilling:* Houston (Schlumberger), document SMP-9160.

Austin, J.A., Jr., Christie-Blick, N., Malone, M.J., et al., 1998. *Proc. ODP, Init. Repts.,* 174A: College Station, TX (Ocean Drilling Program). [**HTML**]

Balsam, W.L., and Damuth, J.E., 2000. Further investigations of shipboard vs. shore-based spectral data: implications for interpreting Leg 164 sediment composition. *In* Paull, C.K., Matsumoto, R., Wallace, P., and Dillon, W.P. (Eds.), *Proc. ODP, Sci. Results,* 164: College Station, TX (Ocean Drilling Program), 313–324. [**HTML**]

Balsam, W.L., Damuth, J.E., and Schneider, R.R., 1997. Comparison of shipboard vs. shore-based spectral data from Amazon Fan cores: implications for interpreting sediment composition. *In* Flood, R.D., Piper, D.J.W., Klaus, A., and Peterson, L.C. (Eds.), *Proc. ODP, Sci. Results,* 155: College Station TX (Ocean Drilling Program), 193–215. [**PDF**]

Balsam, W.L., Deaton, B.C., and Damuth, J.E., 1998. The effects of water content on diffuse reflectance measurements of deep-sea core samples: an example from ODP Leg 164 sediments. *Mar. Geol.,* 149:177–189. **doi:10.1016/S0025-3227(98)00033-4**

Bassinot, F.C., Labeyrie, L.D., Vincent, E., Quidelleur, X., Shackleton, N.J., and Lancelot, Y., 1994. The astronomical theory of climate and the age of the Brunhes-Matuyama magnetic reversal. *Earth Planet. Sci. Lett.,* 126:91–108. **doi:10.1016/0012-821X(94)90244-5**

Berggren, W.A., Hilgen, F.J., Langereis, C.G., Kent, D.V., Obradovich, J.D., Raffi, I., Raymo, M.E., and Shackleton, N.J., 1995. Late Neogene chronology: new perspectives in high-resolution stratigraphy. *Geol. Soc. Am. Bull.,* 107:1272–1287. **doi:10.1130/0016-7606(1995)107<1272:LNCNPI>2.3.CO;2**

Bickert, T., Curry, W.B., and Wefer, G., 1997. Late Pliocene to Holocene (2.6–0 Ma) western equatorial Atlantic deep-water circulation: inferences from benthic stable isotopes. *In* Shackleton, N.J., Curry, W.B., Richter, C., and Bralower, T.J. (Eds.), *Proc. ODP, Sci. Results,* 154: College Station, TX (Ocean Drilling Program), 239–253.

Binns, R.A., Barriga, F.J.A.S., Miller, D.J., et al., 2002. *Proc. ODP, Init. Repts.,* 193 [CD-ROM]. Available from: Ocean Drilling Program, Texas A&M University, College Station TX 77845-9547, USA. [**HTML**]

Bloemendal, J., Lamb, B., and King, J., 1988. Paleoenvironmental implications of rock-magnetic properties of late Quaternary sediment cores from the eastern equatorial Atlantic. *Paleoceanography,* 3:61–87.

Blum, P., 1997. Physical properties handbook: a guide to the shipboard measurement of physical properties of deep-sea cores. *ODP Tech. Note,* 26 [Online]. Available from World Wide Web: <**http://www-odp.tamu.edu/publications/tnotes/tn26/INDEX.HTM**>.

Bolli, H.M., and Saunders, J.B., 1985. Oligocene to Holocene low latitude planktic foraminifera. *In* Bolli, H.M., Saunders, J.B., and Perch-Nielsen, K. (Eds.), *Plankton Stratigraphy:* Cambridge (Cambridge Univ. Press), 155–262.

Boyce, R.E., 1977. Deep Sea Drilling Project procedures for shear strength measurement of clayey sediment using modified Wykeham Farrance laboratory vane apparatus. *In* Barker, P.F., Dalziel, I.W.D., et al., *Init. Repts. DSDP,* 36: Washington (U.S. Govt. Printing Office), 1059–1068.

Brückmann, W., Moran, K., and Housen, B.A., 1997. Directional properties of *P*-wave velocities and acoustic anisotropy in different structural domains of the northern Barbados Ridge accretionary complex. *In* Shipley, T.H., Ogawa, Y., Blum, P., and Bahr, J.M. (Eds.), *Proc. ODP, Sci. Results,* 156: College Station, TX (Ocean Drilling Program), 115–123.

Bukry, D., 1973. Low-latitude coccolith biostratigraphic zonation. *In* Edgar, N.T., Saunders, J.B., et al., *Init. Repts., DSDP,* 15: Washington (U.S. Govt. Printing Office), 685–703.

Bukry, D., 1975. Coccolith and silicoflagellate stratigraphy, northwestern Pacific Ocean, Deep Sea Drilling Project Leg 32. *In* Larson, R.L., Moberly, R., et al., *Init. Repts. DSDP,* 32: Washington (U.S. Govt. Printing Office), 677–701.

Cande, S.C., and Kent, D.V., 1992. A new geomagnetic polarity time scale for the Late Cretaceous and Cenozoic. *J. Geophys. Res.,* 97(10):13917–13951.

Cande, S.C., and Kent, D.V., 1995. Revised calibration of the geomagnetic polarity timescale for the Late Cretaceous and Cenozoic. *J. Geophys. Res.,* 100:6093–6095.

Carlson, R.L., and Christensen, N.I., 1977. Velocity anisotropy and physical properties of deep-sea sediments from the western South Atlantic. *In* Supko, P.R., Perch-Nielsen, K., et al., *Init. Repts. DSDP,* 39: Washington (U.S. Govt. Printing Office), 555–559.

Davis, E.E., Mottl, M.J., Fisher, A.T., et al., 1992. *Proc. ODP, Init. Repts.,* 139: College Station, TX (Ocean Drilling Program).

Davis, E.E., Villinger, H., MacDonald, R.D., Meldrum, R.D., and Grigel, J., 1997. A robust rapid-response probe for measuring bottom-hole temperatures in deep-ocean boreholes. *Mar. Geophys. Res.,* 19(3):267–281. **doi:10.1023/A:1004292930361**

DeLong, E.F, 2004. Microbiology: microbial life breathes deep. *Science,* 306:2198–2200. **doi:10.1126/science.1107241**

deMenocal, P., Bloemendal, J., and King, J., 1991. A rock-magnetic record of monsoonal dust deposition to the Arabian Sea: evidence for a shift in the mode of deposition at 2.4 Ma. *In* Prell, W.L., Niitsuma, N., et al., *Proc. ODP, Sci. Results,* 117: College Station, TX (Ocean Drilling Program), 389–407.

D'Hondt, S.D., Jørgensen, B.B., Miller, D.J., Batzke, A., Blake, R., Cragg, B.A., Cypionka, H., Dickens, G.R., Ferdelman, T., Hinrichs, K.-H., Holm, N.G., Mitterer, R., Spivack, A., Wang, G., Bekins, B., Engelen, B., Ford, K., Gettemy, G., Rutherford, S.D., Sass, H., Skilbeck, C.G., Aiello, I.W., Guerin, G., House, C., Inagak, F., Meister, P., Naehr, T., Niitsuma, S., Parkes, R.J., Schippers, A., Smith, D.C., Teske, A., Wiegel, J., Naranjo Padillo, C., and Solis Acosta, J.L., 2004. Distributions of microbial activities in deep subseafloor sediments. *Science,* 306:2216–2221. **doi:10.1126/science.1101155**

Frederichs, T., Bleil, U., Däumler, K., von Dobeneck, T., and Schmidt, A.M., 1999. The magnetic view on the marine paleoenvironment: parameters, techniques, and potentials of rock magnetic studies as a key to paleoclimatic and paleoceanographic changes. *In* Fischer, G., and Wefer, G. (Eds.), *Use of Proxies in Paleoceanography: Examples from the South Atlantic:* Berlin (Springer-Verlag), 575–599.

Gieskes, J.M., Gamo, T., and Brumsack, H., 1991. Chemical methods for interstitial water analysis aboard *JOIDES Resolution*. *ODP Tech. Note,* 15 [Online]. Available from World Wide Web: <**http://www-odp.tamu.edu/publications/tnotes/tn15/f_chem1.htm**>.

Graber, K.K., Pollard, E., Jonasson, B., and Schulte, E. (Eds.), 2002. Overview of Ocean Drilling Program Engineering Tools and Hardware. *ODP Tech. Note,* 31 [Online]. Available from World Wide Web: <**http://www-odp.tamu.edu/publications/tnotes/tn31/INDEX.HTM**>.

Heeseman, M., 2002. Modeling and analysis of transient pressure measurements in ODP boreholes for undisturbed formation pressure estimation [Diplomarbeit im Fach Geophysik]. Univ. Bremen, Germany.

Hine, H., and Weaver, P.P.E., 1998. Quaternary. *In* Bown, P.R. (Ed.), *Calcareous Nannofossil Biostratigraphy:* Dordrecht, The Netherlands (Kluwer Academic Publ.), 266–283.

Holtz, R.D., and Kovacs, W.D., 1981. *An Introduction to Geotechnical Engineering:* Englewood Cliffs, NJ (Prentice-Hall).

Kelemen, P.B., Kikawa, E., Miller, D.J., et al., 2004. *Proc. ODP, Init. Repts.,* 209 [CD-ROM]. Available from: Ocean Drilling Program, Texas A&M University, College Station TX 77845-9547, USA. [**HTML**]

Kennett, J.P., and Huddlestun, P., 1972. Late Pleistocene paleoclimatology, foraminiferal biostratigraphy, and tephrochronology, western Gulf of Mexico. *Quat. Res.,* 2:38–69. **doi:10.1016/0033-5894(72)90004-X**

Kent, D.V., 1982. Apparent correlation of paleomagnetic intensity and climatic records in deep-sea sediments. *Nature (London, U. K.),* 299:538–539. **doi:10.1038/299538a0**

Kimura, G., Silver, E.A., Blum, P., et al., 1997. *Proc. ODP, Init. Repts.,* 170: College Station, TX (Ocean Drilling Program). [**HTML**]

Kristiansen, J.I., 1982. The transient cylindrical probe method for determination of thermal parameters of earth materials [Ph.D. dissert.]. Åarhus Univ.

Mackenzie, K.V., 1981. Nine-term equation for sound speed in the oceans. *J. Acoust. Soc. Am.,* 70:807–812. **doi:10.1121/1.386920**

Martin, R.E., Johnson, G.W., Neff, E.D., and Krantz, D.W., 1990. Quaternary planktonic foraminiferal assemblage zones of the northeast Gulf of Mexico, Columbia basin (Caribbean Sea), and tropical Atlantic Ocean: graphic correlation of microfossil and oxygen isotope datums. *Paleoceanography,* 5:531–555.

Martini, E., 1971. Standard Tertiary and Quaternary calcareous nannoplankton zonation. *In* Fainacci, A. (Ed.), *Proc. 2nd Int. Conf. Planktonic Microfossils Roma:* Rome (Ed. Tecnosci.), 2:739–785.

Martini, E., and Müller, C., 1986. Current Tertiary and Quaternary calcareous nannoplankton stratigraphy and correlations. *Newsl. Stratigr.,* 16:99–112.

Mazzullo, J., and Graham, A.G. (Eds.), 1988. Handbook for shipboard sedimentologists. *ODP Tech. Note,* 8.

Mikada, H., Becker, K., Moore, J.C., Klaus, A., et al., 2002. *Proc. ODP, Init. Repts.,* 196 [CD-ROM]. Available from: Ocean Drilling Program, Texas A&M University, College Station TX 77845-9547, USA. [**HTML**]

Moore, J.C., Klaus, A., et al., 1998. *Proc. ODP, Init. Repts.,* 171A [CD-ROM]. Available from: Ocean Drilling Program, Texas A&M University, College Station, TX 77845-9547, U.S.A. [**HTML**]

O'Brien, P.E., Cooper, A.K., Richter, C., et al., 2001. *Proc. ODP, Init. Repts.,* 188 [CD-ROM]. Available from: Ocean Drilling Program, Texas A&M University, College Station TX 77845-9547, USA. [**HTML**]

Perch-Nielsen, K., 1985. Cenozoic calcareous nannofossils. *In* Bolli, H.M., Saunders, J.B., and Perch-Nielsen, K. (Eds.), *Plankton Stratigraphy:* Cambridge (Cambridge Univ. Press), 427–554.

Pimmel, A., and Claypool, G., 2001. Introduction to shipboard organic geochemistry on the *JOIDES Resolution*. *ODP Tech. Note,* 30 [Online]. Available from World Wide Web: <**http://www-odp.tamu.edu/publications/tnotes/tn30/INDEX**>.

Poag, C.W., 1981. *Ecologic Atlas of Benthic Foraminifera of the Gulf of Mexico:* Stroudsburg, PA (Hutchinson Ross).

Pribnow, D.F.C., Kinoshita, M., and Stein, C.A., 2000. Thermal data collection and heat flow recalculations for ODP Legs 101–180. Institute for Joint Geoscientific Research, GGA, Hanover, Germany, 0120432. Available from World Wide Web: <**http://www-odp.tamu.edu/publications/heatflow/ODPReprt.pdf**>.

Radhakrishnamurty, C., Likhite, S.D., Amin, B.S., and Somayajulu, B.L.K., 1968. Magnetic susceptibility stratigraphy in ocean sediment cores. *Earth Planet. Sci. Lett.,* 4:464–468. **doi:10.1016/0012-821X(68)90025-3**

Robinson, S.G., 1986. The late Pleistocene paleoclimatic record of North Atlantic deep-sea sediments revealed by mineral-magnetic measurements. *Phys. Earth Planet. Inter.,* 42(1–2):22–47. **doi:10.1016/S0031-9201(86)80006-1**

Schlumberger, 1994. *Log Interpretation Charts:* Sugarland, TX (Schlumberger Wireline and Testing), SMP-7006.

Shepard, F.P., 1954. Nomenclature based on sand-silt-clay ratios. *J. Sediment. Petrol.,* 24:151–158.

Shipboard Scientific Party, 1992. Explanatory notes. *In* Mayer, L., Pisias, N., Janecek, T., et al., *Proc. ODP, Init. Repts.,* 138 (Pt. 1): College Station, TX (Ocean Drilling Program), 13–42.

Shipboard Scientific Party, 1999. Explanatory notes. *In* Gersonde, R., Hodell, D.A., Blum, P., et al., *Proc. ODP, Init. Repts.,* 177, 1–57 [CD-ROM]. Available from: Ocean Drilling Program, Texas A&M University, College Station, TX 77845-9547, U.S.A. [**HTML**]

Shipboard Scientific Party, 2000. Explanatory notes. *In* Wang, P., Prell, W.L., Blum, P., et al., *Proc. ODP, Init. Repts.,* 184, 1–48 [CD-ROM]. Available from: Ocean Drilling Program, Texas A&M University, College Station TX 77845-9547, USA. [**HTML**]

Shipboard Scientific Party, 2003. Explanatory notes. *In* Tréhu, A.M, Bohrmann, G., Rack, F.R., Torres, M.E., et al., *Proc. ODP, Init. Repts.,* 204, 1–102 [CD-ROM]. Available from: Ocean Drilling Program, Texas A&M University, College Station TX 77845-9547, USA. [**HTML**]

Shipboard Scientific Party, 2004. Explanatory notes. *In* Zachos, J.C., Kroon, D., Blum, P., et al., *Proc. ODP, Init. Repts.,* 208, 1–63 [CD-ROM]. Available from: Ocean Drilling Program, Texas A&M University, College Station TX 77845-9547, USA. [**HTML**]

Shipley, T.H., Ogawa, Y., Blum, P., et al., 1995. *Proc. ODP, Init. Repts.,* 156: College Station, TX (Ocean Drilling Program).

Smith, D.C., Spivack, A.J., Fisk, M.R., Haveman, S.A., Staudigel, H., and ODP Leg 185 Shipboard Scientific Party, 2000. Methods for quantifying potential microbial contamination during deep ocean coring. *ODP Tech. Note,* 28 [Online]. Available from World Wide Web: <**http://www-odp.tamu.edu/publications/tnotes/tn28/INDEX.HTM**>.

Takayama, T., and Sato, T., 1987. Coccolith biostratigraphy of the North Atlantic Ocean, Deep Sea Drilling Project Leg 94. *In* Ruddiman, W.F., Kidd, R.B., Thomas, E., et al., *Init. Repts. DSDP,* 94 (Pt. 2): Washington (U.S. Govt. Printing Office), 651–702.

Terry, R.D., and Chilingar, G.V., 1955. Summary of "Concerning some additional aids in studying sedimentary formations" by M.S. Shvetsov. *J. Sediment. Petrol.,* 25:229–234.

Tréhu, A.M., Bohrmann, G., Rack, F.R., Torres, M.E., et al., 2003. *Proc. ODP, Init. Repts.,* 204 [CD-ROM]. Available from: Ocean Drilling Program, Texas A&M University, College Station TX 77845-9547, USA. [**HTML**]

van Morkhoven, F.P.C.M., Berggren, W.A., and Edwards, A.S., 1986. *Cenozoic Cosmopolitan Deep-Water Benthic Foraminifera.* Bull. Cent. Rech. Explor.—Prod. Elf-Aquitaine, Mem. 11.

von Dobeneck, T., and Schmieder, F., 1999. Using rock magnetic proxy records for orbital tuning and extended time series analysis into the super- and sub-Milankovitch bands. *In* Fischer, G., and Wefer, G. (Eds.), *Use of Proxies in Paleoceanography: Examples from the South Atlantic:* Heidelberg (Springer-Verlag), 601–633.

Von Herzen, R.P., and Maxwell, A.E., 1959. The measurement of thermal conductivity of deep-sea sediments by a needle-probe method. *J. Geophys. Res.,* 64:1557–1563.

Wentworth, C.K., 1922. A scale of grade and class terms of clastic sediments. *J. Geol.,* 30:377–392.

Whitman, W.B., Coleman, D.C., and Wiebe, W.J., 1998. Prokaryotes: the unseen majority. *Proc. Natl. Acad. Sci. U.S.A.,* 95:6578–6583. **doi:10.1073/pnas.95.12.6578**

Whittle, A.J., Sutabutr, T., Germaine, J.T., and Varney, A., 2001. Prediction and measurement of pore pressure dissipation for a tapered piezocone. *Geotechnique,* 51:601–617.

Wilson, W.D., 1960. Speed of sound in seawater as a function of temperature, pressure and salinity. *J. Acoust. Soc. Am.,* 32(6):641–644. **doi:10.1121/1.1908167**

Wyllie, M.R.J., Gregory, A.R., and Gardner, L.W., 1956. Elastic wave velocities in heterogeneous and porous media. *Geophysics,* 21(1):41–70. **doi:10.1190/1.1438217**

Publication: 8 July 2006
MS 308-102

Figure F1. Grain size classification of Wentworth (1922).

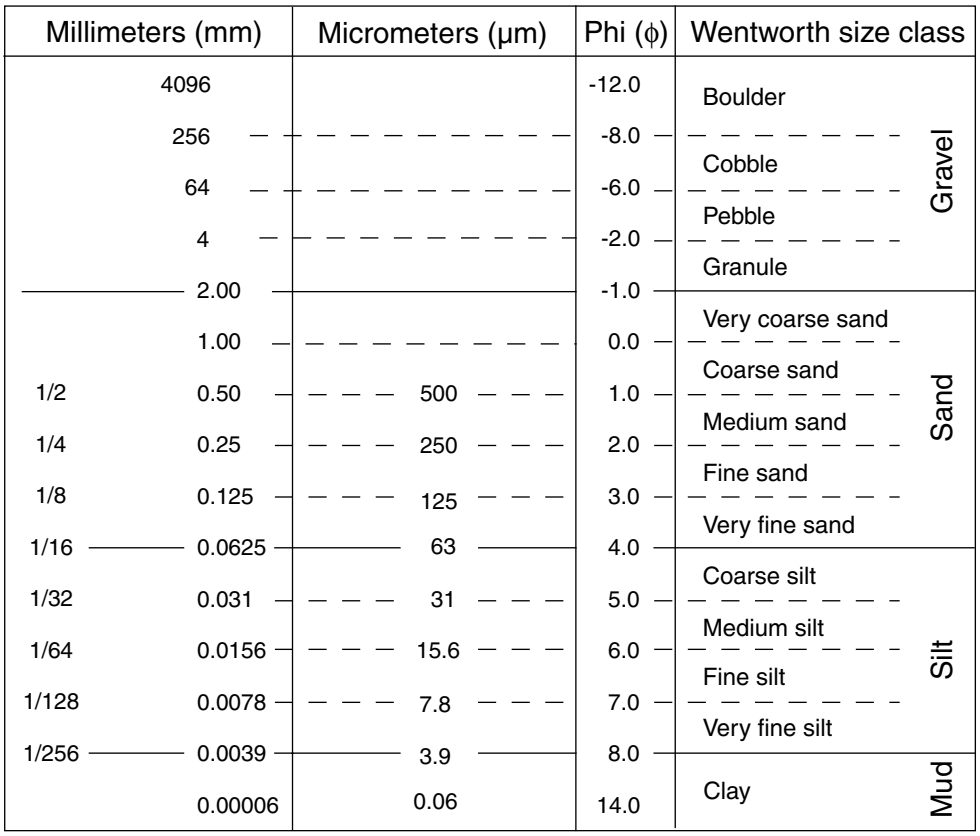

Figure F2. Ternary diagram for naming siliciclastic sediments, modified from Shepard (1954).

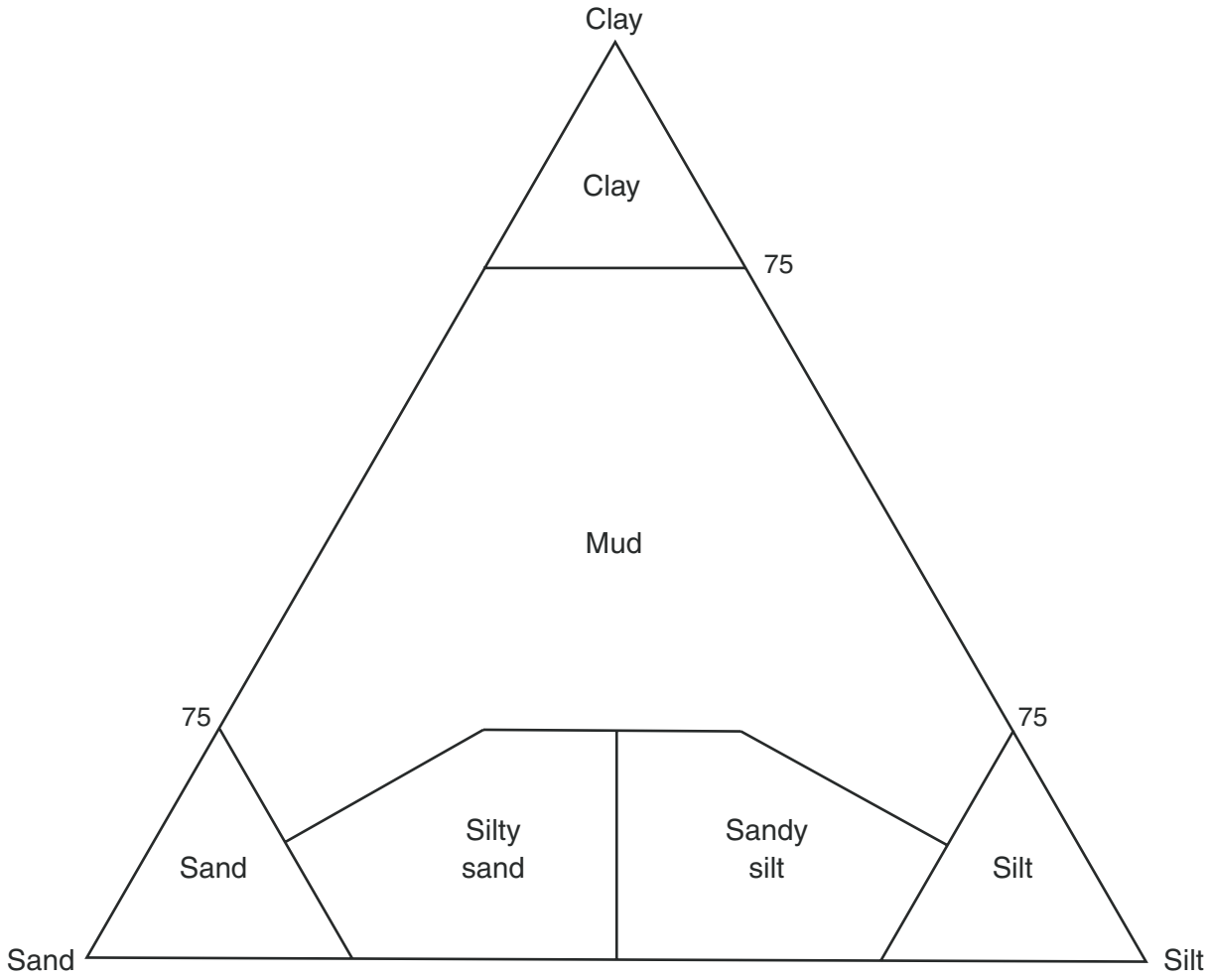

Figure F3. Example of visual core description (VCD) form. IW = interstitial water, WHC = whole-round core sample.

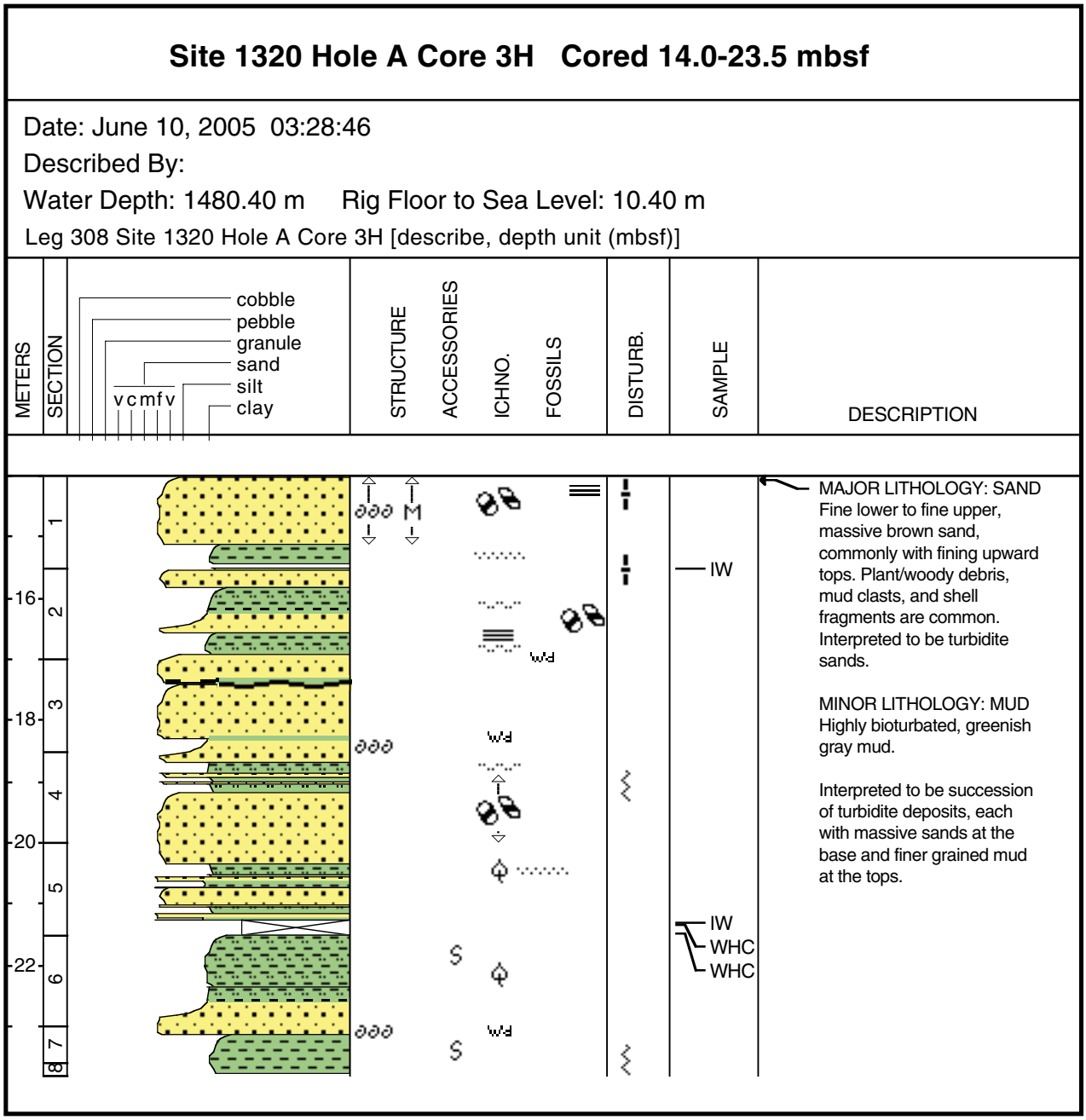

Figure F4. Legend for symbols used in the visual core description forms.

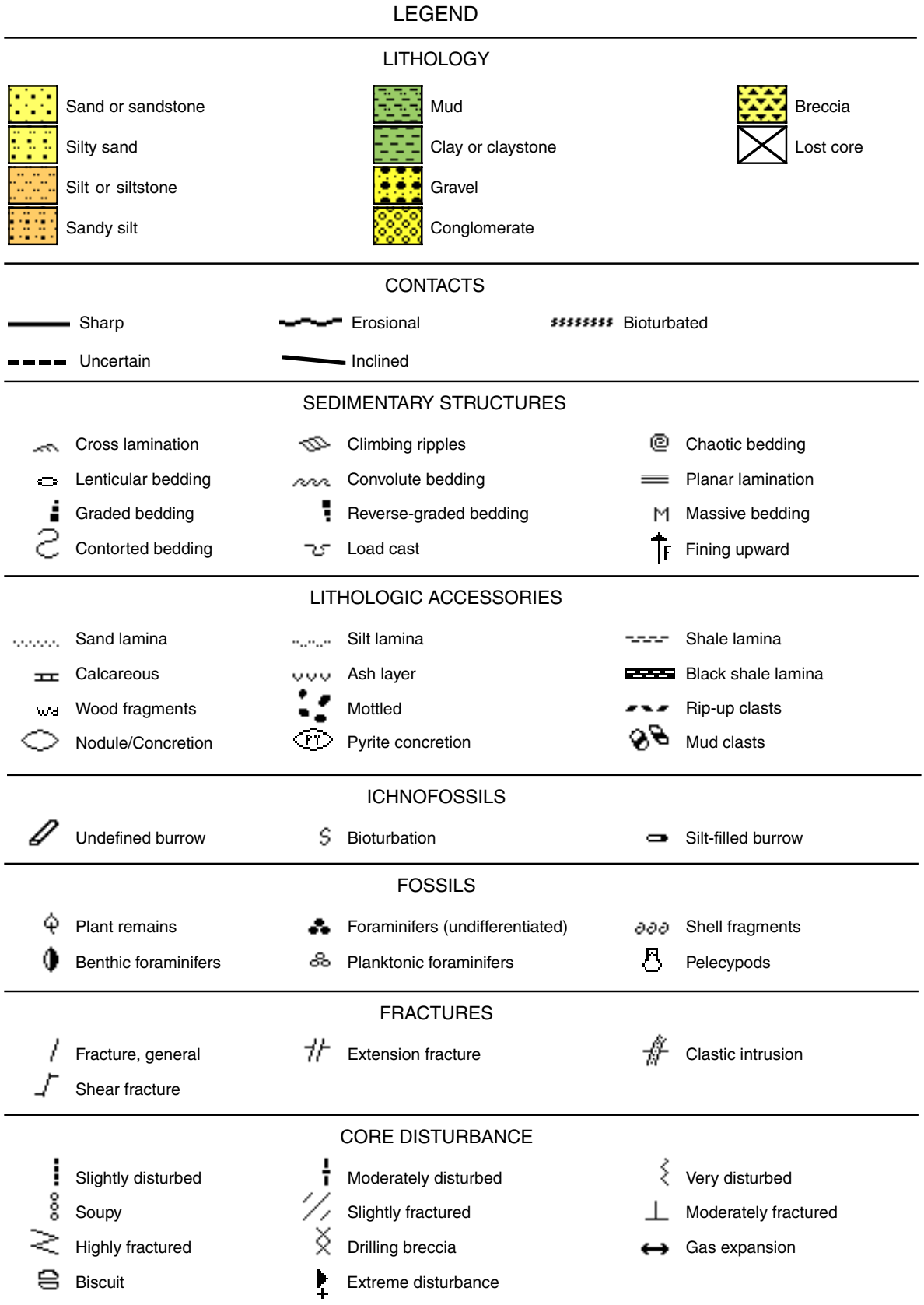

Figure F5. Chronostratigraphy of Berggren et al. (1995) showing the correlation of planktonic foraminifer (PF; blue) and nannofossil (N; green) zones and species datum levels. FO = first occurrence, LO = last occurrence.

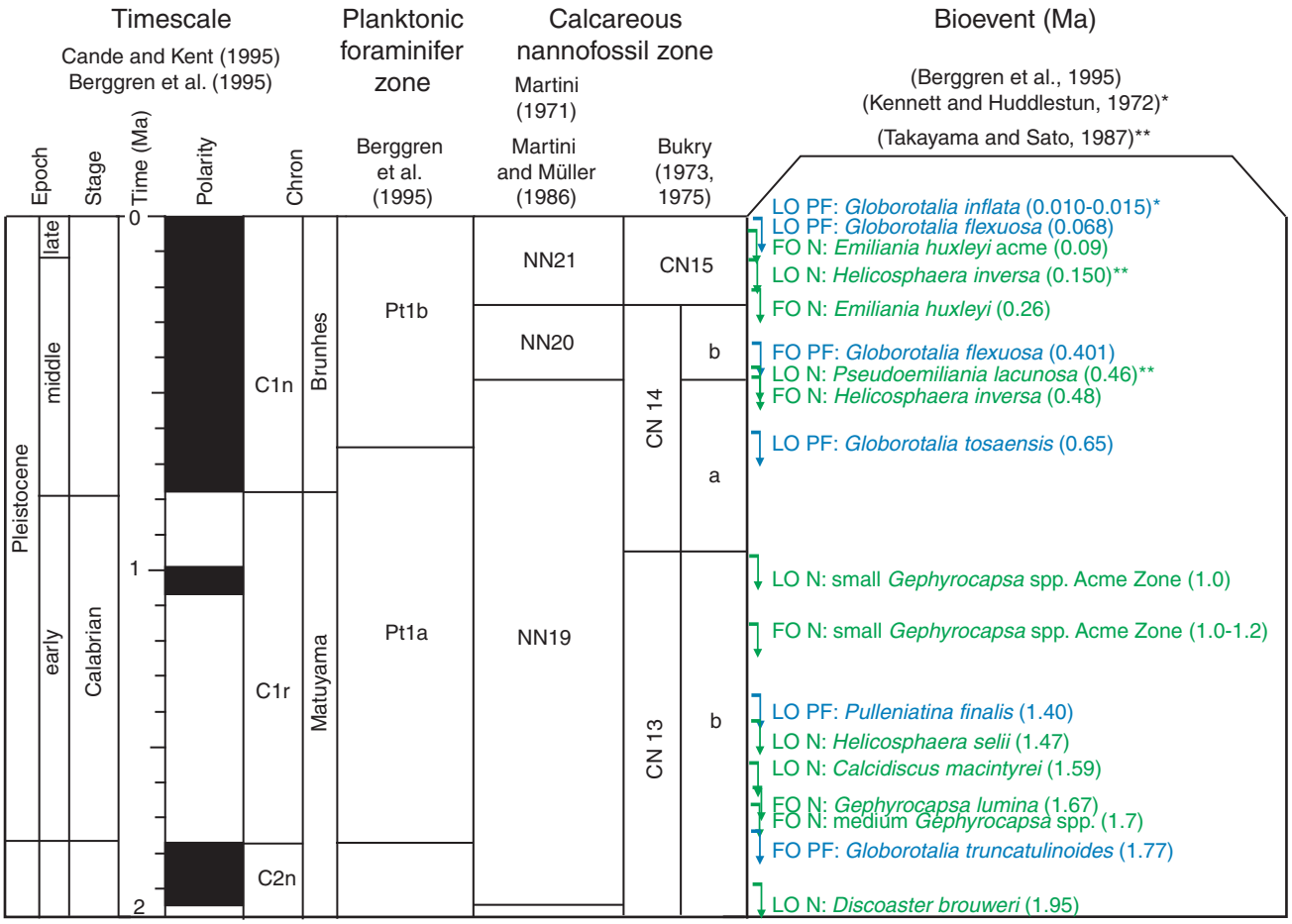

Figure F6. Acme intervals determined from Deep Sea Drilling Project (DSDP) Site 610 (Hole 610B). Graphs refer to percentage relative abundance of nannoplankton species (after Hine and Weaver, 1998).

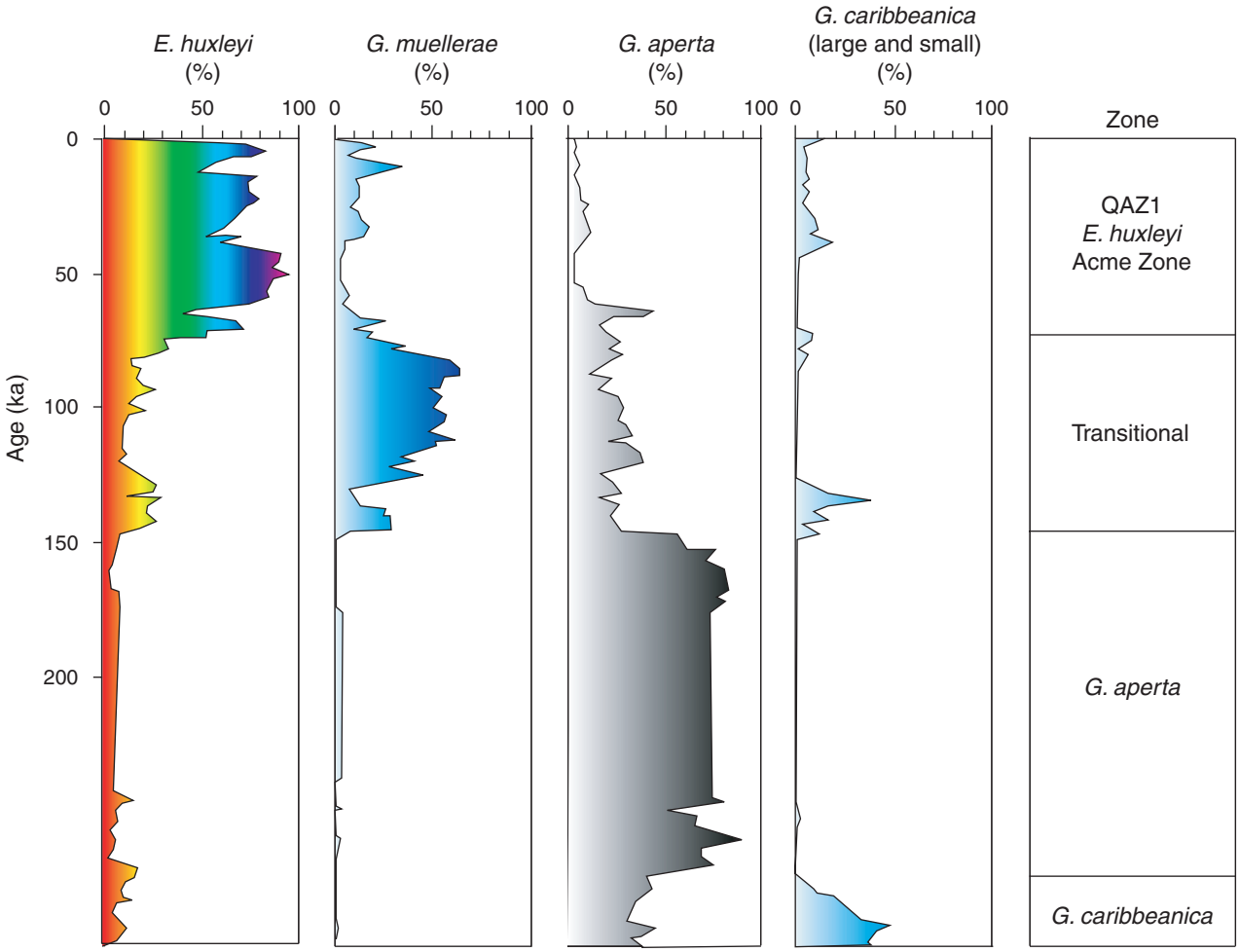

Figure F7. Low-latitude oxygen isotopic stack for the late Quaternary, showing marine isotope stages (MIS) and events (Bassinot et al., 1994). Planktonic foraminifer assemblage zones and subzones as well as ash layers (stars) from the Gulf of Mexico are after Kennett and Huddlestun (1972), with boundary ages adjusted using low-latitude MIS events (Bassinot et al., 1994). Purple text stands for planktonic foraminifer datum and green text stands for nannofossil datum.

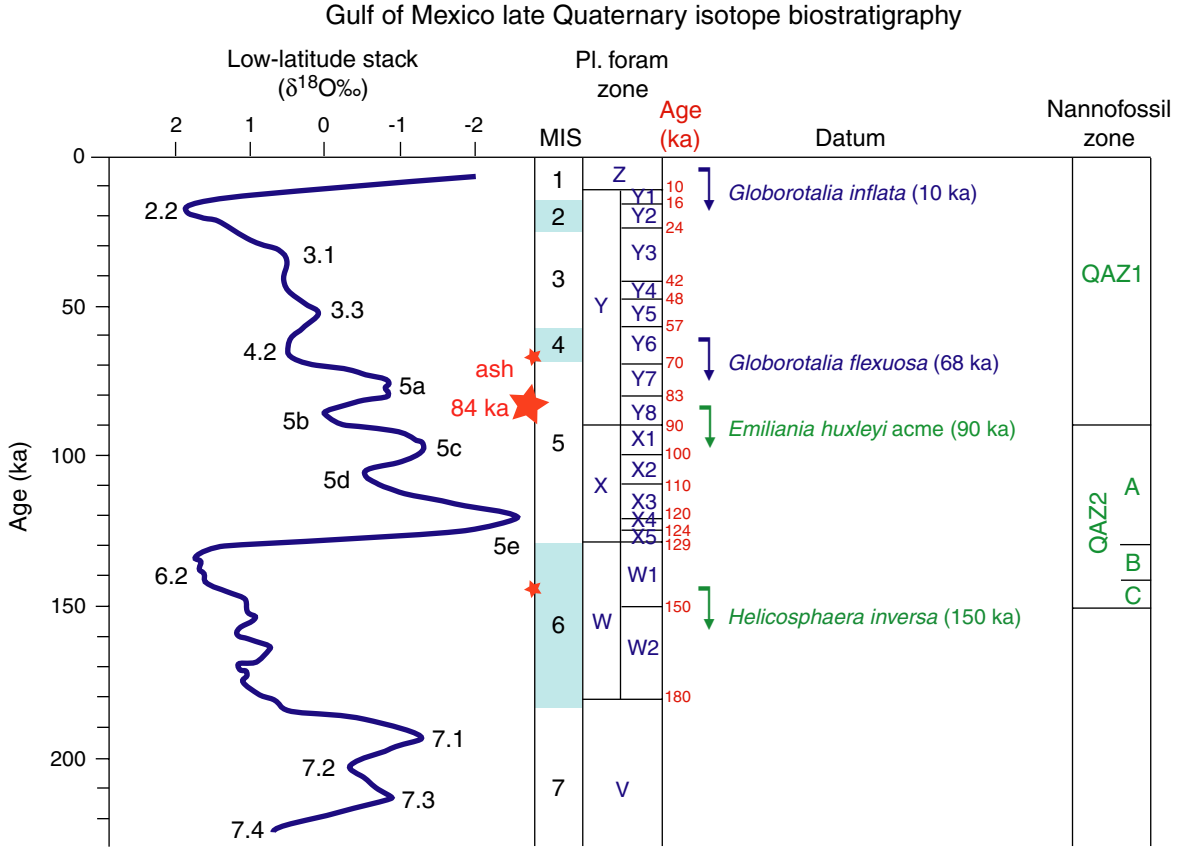

Figure F8. Core flow chart in the core laboratory. MST = multisensor track: GRA = gamma ray attenuation (density), PWL = *P*-wave logger (velocity), MSL = magnetic susceptibility logger, NCR = noncontact resistivity. MAD = moisture and density.

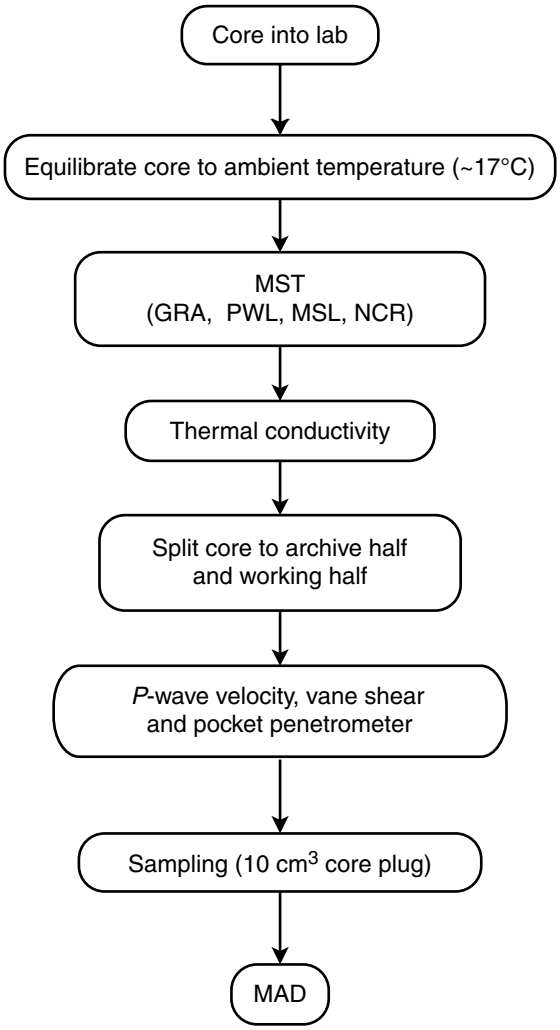

Figure F9. Definition of axis orientation on working-half sections. The z-axis is positive in the downhole direction of the core orientation.

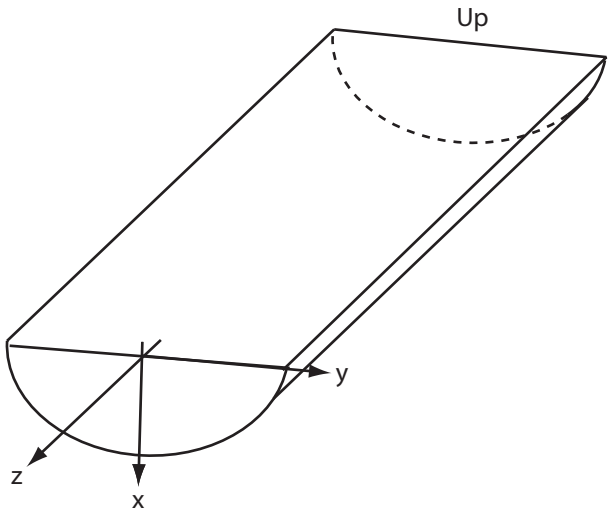

Figure F10. Diagram of the temperature/dual pressure (T2P) probe. **A.** T2P probe with narrow, straight needle shaft. **B.** T2P probe with narrow, tapered needle shaft.

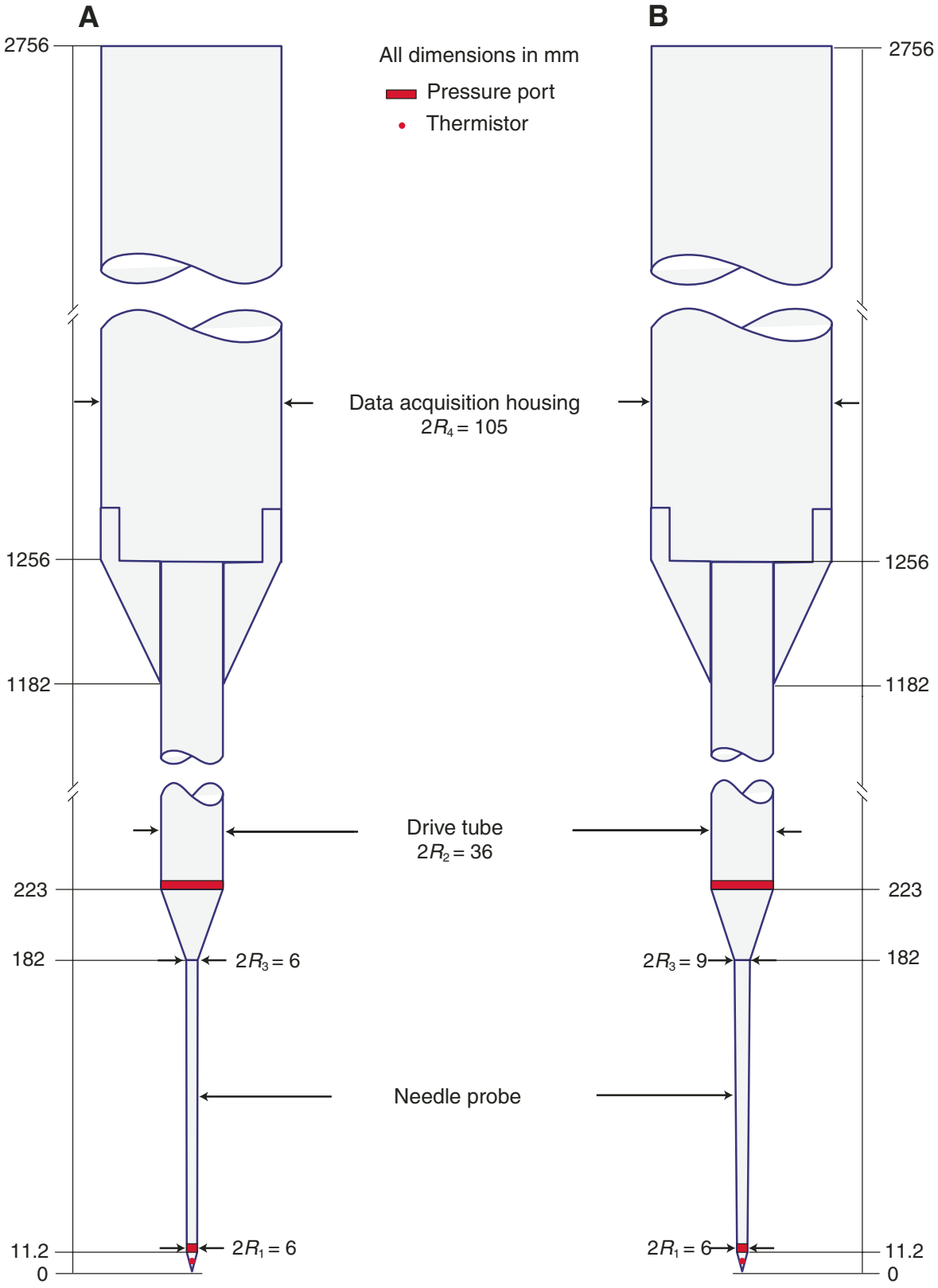

Figure F11. Configuration of the drill string used for logging-while-drilling (LWD) operations. VDN = Vision Neutron Density tool, PowerPulse = Measurement-While-Drilling tool, ARC = Array Resistivity Compensated tool, and GVR = GeoVision Resistivity tool.

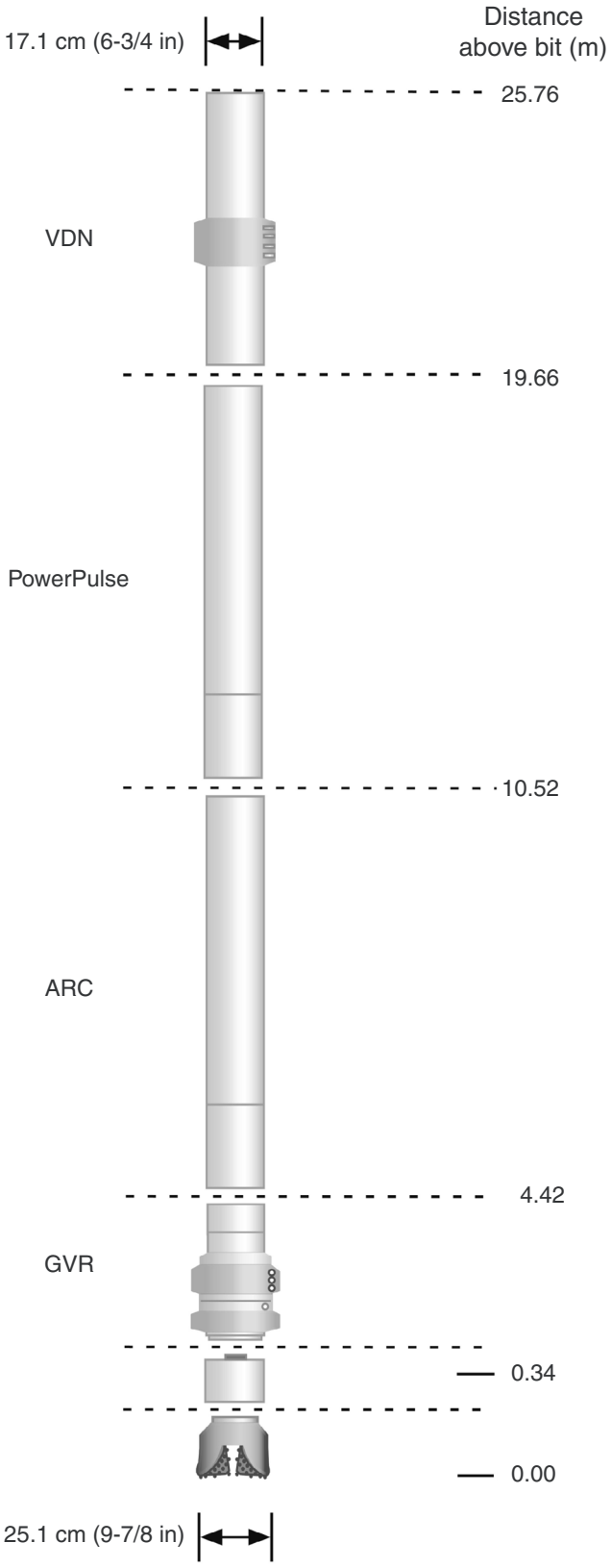

Figure F12. Schematic figure of rig instrumentation. DWOB = downhole weight on bit, DTOR = downhole weight on torque, APWD = annular pressure while drilling, ECD = equivalent circulating density, TEMP = temperature.

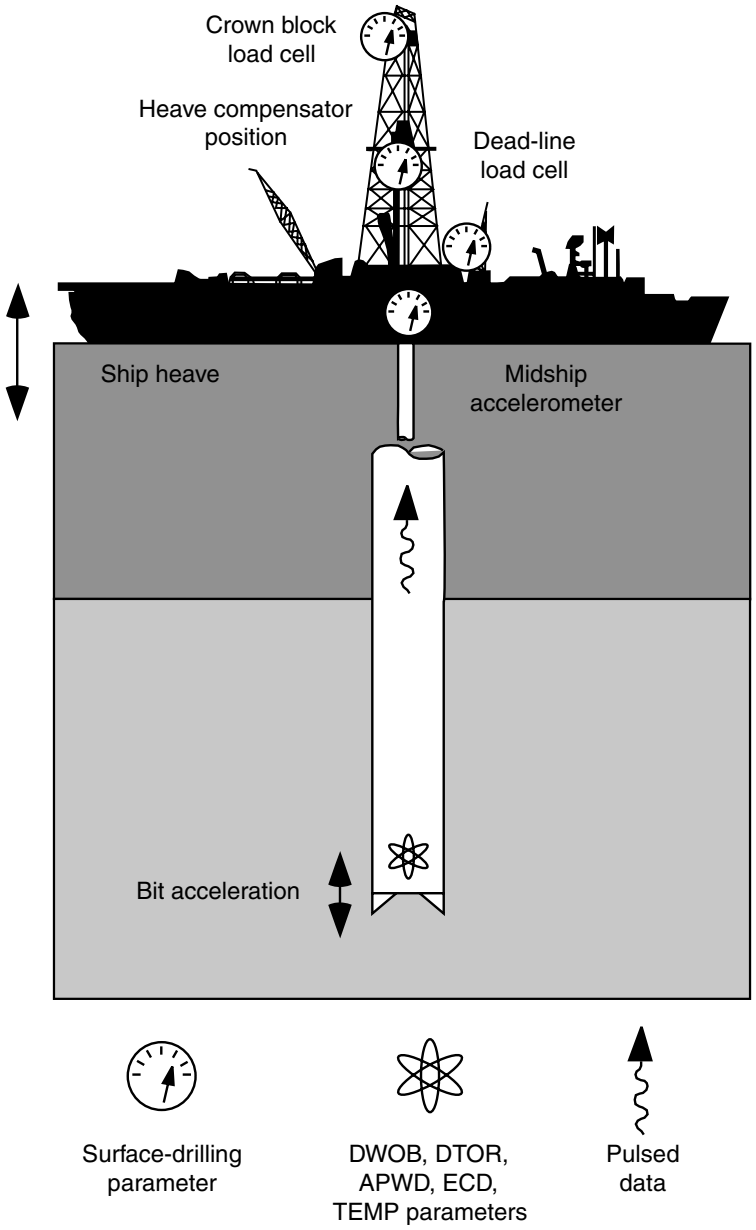

Figure F13. Schematic illustration of the GeoVision Resistivity (GVR) tool. BS = button resistivity shallow, BM = button resistivity medium, BD = button resistivity deep, RING = ring resistivity, GR = gamma radiation.

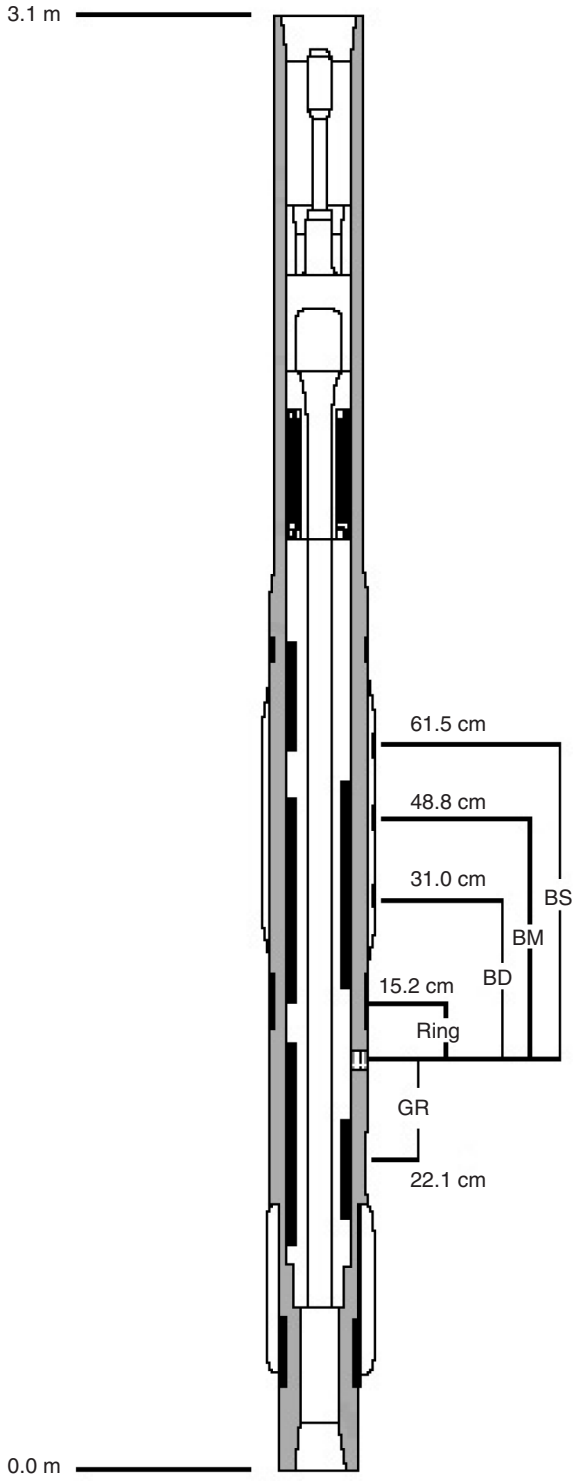

GeoVision Resistivity (GVR) tool

Resistivity measurement specifications
Accuracy: ~5%
Range: 0.2 - 250 Ωm
Vertical resolution
- RES_BIT: 31 - 61 cm
- RES_RING: 8 - 10 cm
- RES_BS: 5 - 8 cm
- RES_BM: 5 - 8 cm
- RES_BD: 5 - 8 cm

Depth of investigation
- RES_BIT: 81 cm
- RES_RING: 56 - 64 cm
- RES_BS: 48 - 61 cm
- RES_BM: 38 - 53 cm
- RES_BD: 28 - 41 cm

Gamma ray measurement specifications
Accuracy: ±7%
Range: 0 - 250 gAPI
Statistical repeatability:
±2% 1 @ 100 gAPI, 30 m/h with 46 cm averaging

Figure F14. Schematic illustration of the Array Resistivity Compensated (ARC) tool.

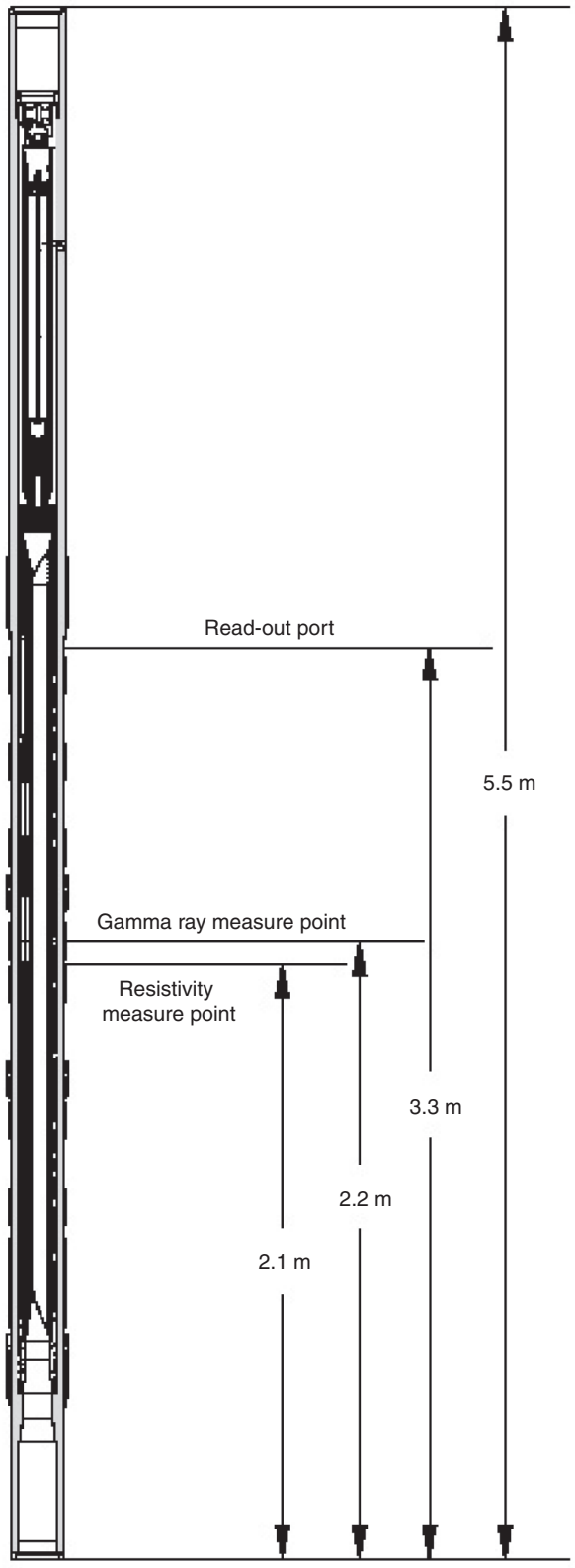

Array Resistivity Compensated (ARC) tool

Resistivity measurement specifications
Accuracy: ~2%
Range: 0.2 - 60 Ωm
Vertical resolution: 21 - 31 cm
Depth of investigation: 33 - 76 cm

Gamma ray measurement specifications
Accuracy: ~3%
Range: 0 - 250 gAPI
Vertical resolution: 15 cm
Statistical repeatability:
±2 at 100 gAPI and 30 m/h 3-pt average

Figure F15. Schematic illustration of the MWD PowerPulse tool.

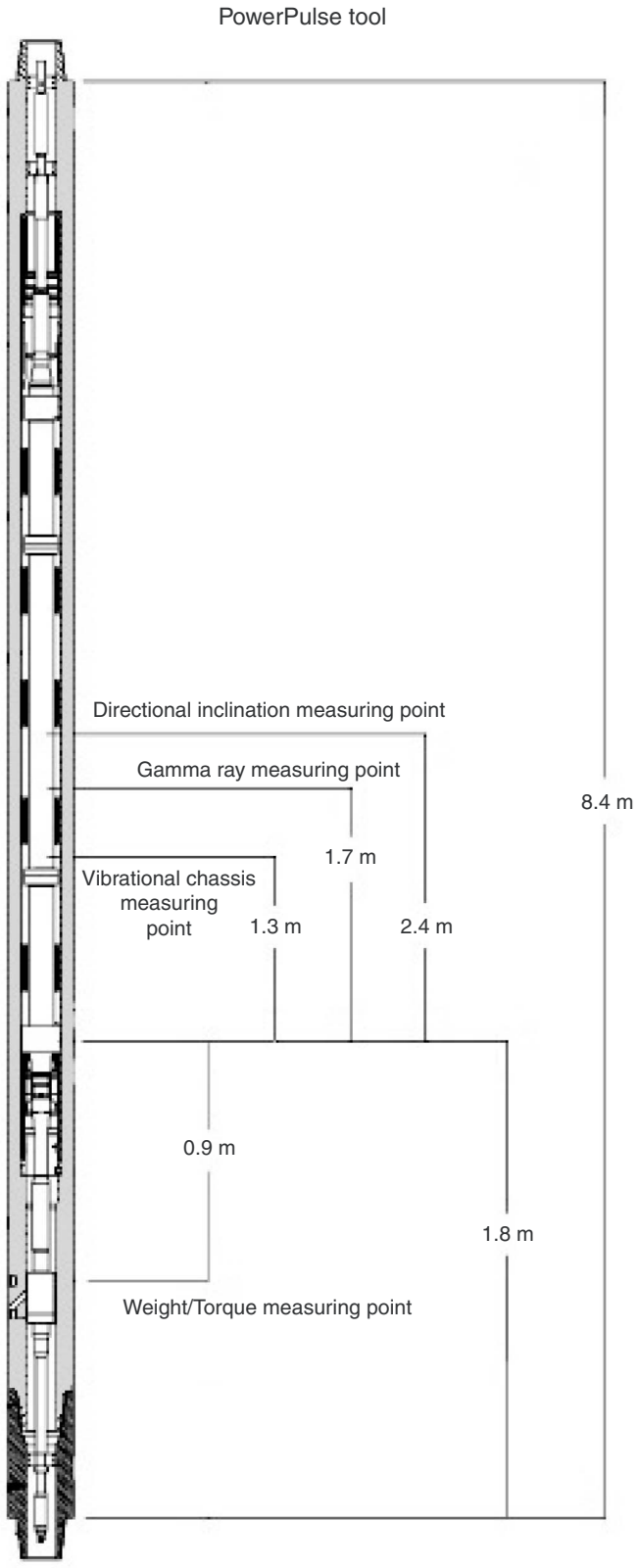

Figure F16. Schematic illustration of the MWD operation method. Drilling fluids are constantly pumped down the drill string, and periodic closure of the MWD valve creates pressure pulses that can be detected on the rig floor.

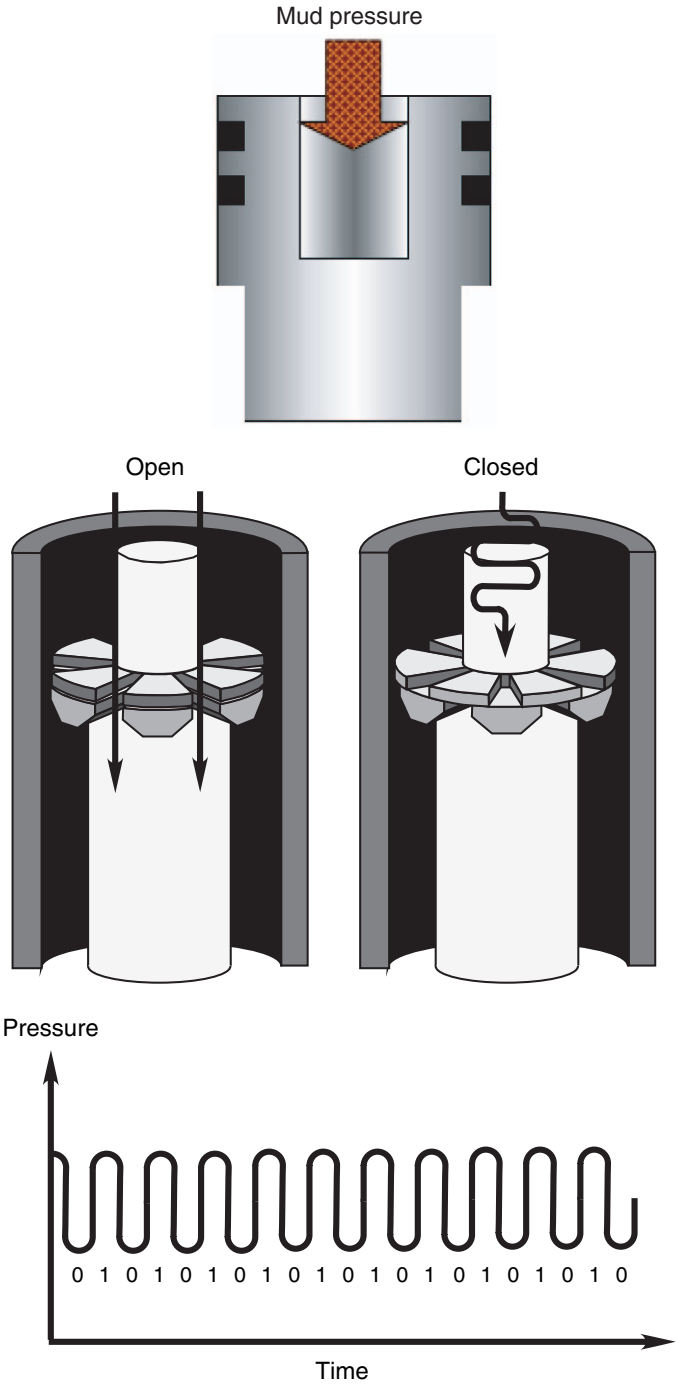

Figure F17. Schematic illustration of the Vision Density Neutron tool. PEF = photoelectric factor.

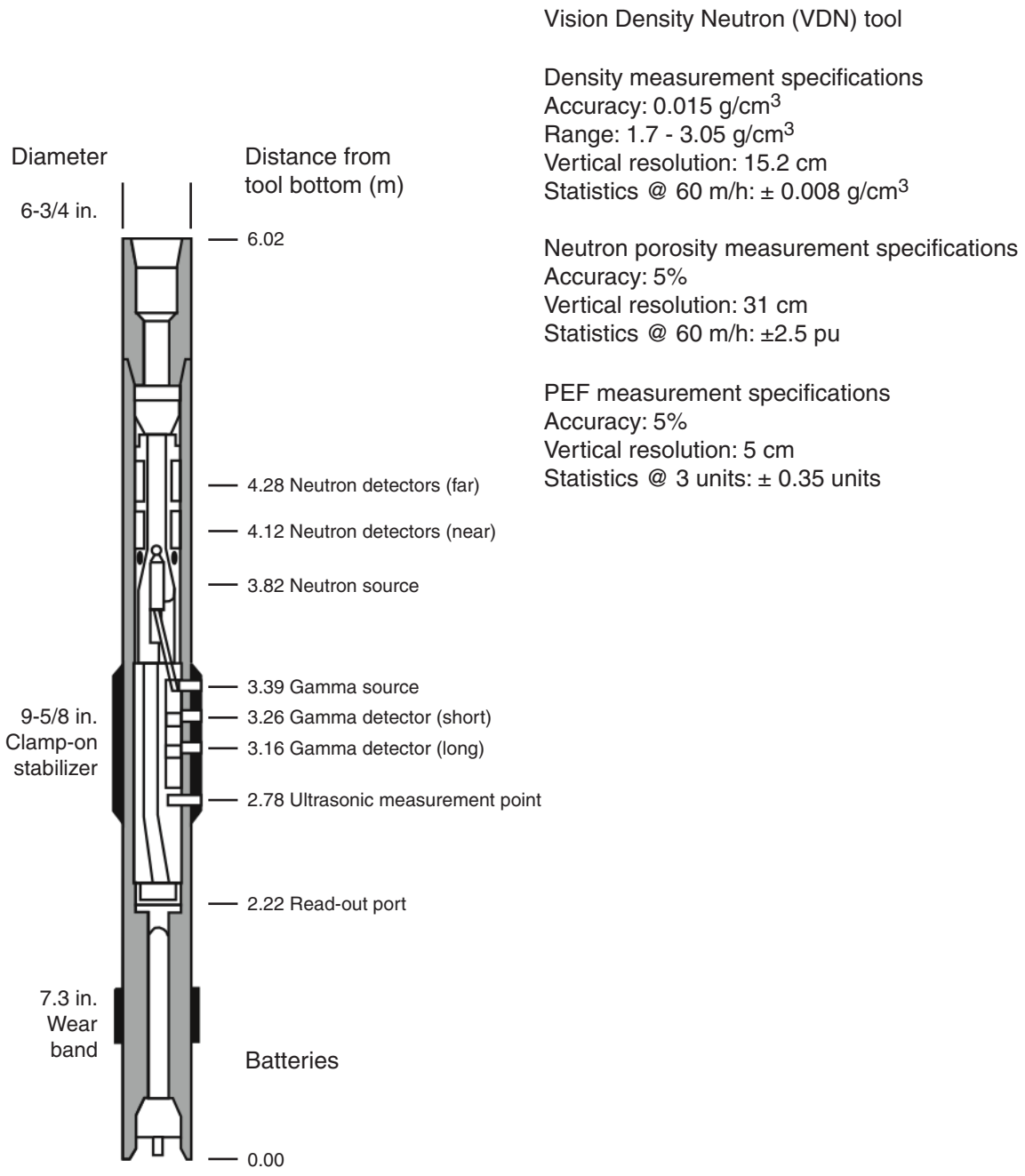

Figure F18. Configuration of the tool strings used for wireline logging operations. See Tables **T3** and **T4** for names of tool strings.

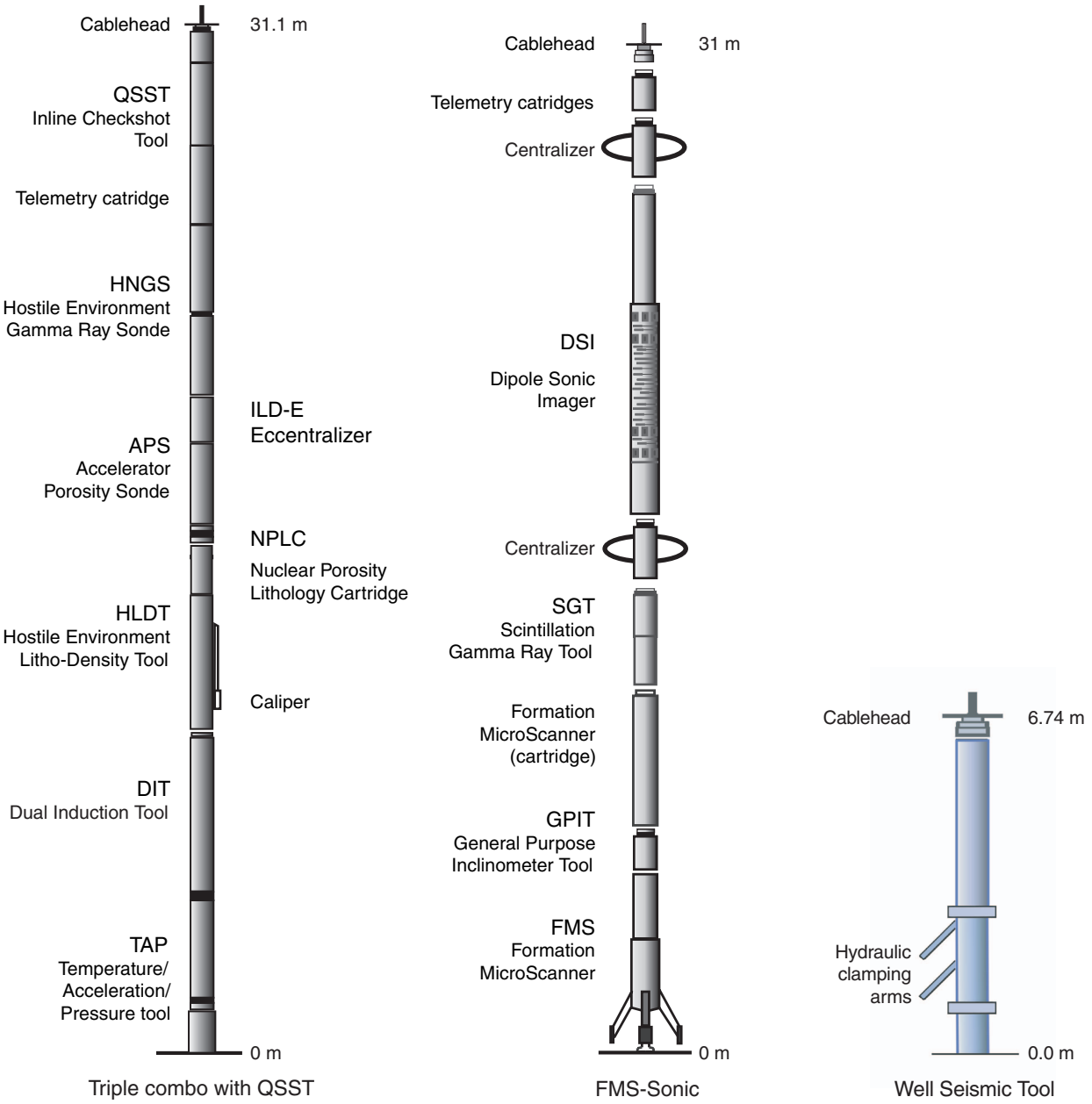

Table T1. Acronyms and units used for wireline logging tools.

Tool	Output	Tool name/Data point description	Unit
VDN		VISION Density Neutron	
	TNPH	Thermal neutron porosity	%
	IDRO	Image derived density	g/cm^3
	RHOB (L,R,U,B)	Bulk density (left, right, up, bottom)	g/cm^3
	IDDR	Image derived density correction	g/cm^3
	DRHO (L,R,U,B)	Bulk density correction (left, right, up, bottom)	g/cm^3
	DCAV	Density caliper	inch
	IDPE	Image-derived photoelectric factor	—
	PE (L,R,U,B)	Photoelectric factor (left, right, up, bottom)	—
PowerPulse		PowerPulse	
	DTOR_RT	Real-time downhole torque	kft·lb
	DWOB_RT	Real-time downhole weight on bit	klbf
	VIBTOR_RT	Real-time downhole torque	ft/lb
	TRPM_RT	Real-time powerpulse turbine rpm	rpm
	SHKPK_RT	Real-time powerpulse peak shock	G
	SHKRSK_RT	Real-time powerpulse shock risk	—
	STICK_RT	Real-time powerpulse peak to peak collar RPM Variation	rpm
	CRPM_RT	Real-time powerpulse collar RPM	rpm
ARC		Array Resistivity Compensated	
	GR_ARC_UNC	ARC uncorrected gamma ray	gAPI
	PxxB	ARC blended phase resistivity xx inches	Ωm
	AxxB	ARC blended attenuation resistivity xx inches	Ωm
	PxxH	ARC phase resistivity xx inches at 2 MHz	Ωm
	AxxH	ARC attenuation resistivity xx inches at 2 MHz	Ωm
	PxxL	ARC phase resistivity xx inches at 400 kHz	Ωm
	AxxL	ARC attenuation resistivity xx inches at 400 kHz	Ωm
	APRS	ARC annulus pressure	psi
	ATMP	ARC annulus temperature	°C
	ECD_ARC	ARC equivalent circulating density	ppg
GVR		GeoVISION Resistivity	
	GR_RAB	GVR gamma ray	gAPI
	RES_BS	GVR shallow button resistivity	Ωm
	RES_BM	GVR medium button resistivity	Ωm
	RES_BD	GVR deep button resistivity	Ωm
	RES_RING	GVR ring resistivity	Ωm
	RES_BIT	GVR bit resistivity	Ωm
	RPM_RAB	GVR rotational speed	rpm
	AAI	GVR angular acceleration indicator	—

Table T2. Correction factors for GVR tool.

Measurement	Correction factor (%)
Resistivity-at-the-bit	3
Ring resistivity	1
Deep resistivity	2
Medium resistivity	4
Shallow resistivity	NA

Note: NA = not applicable.

Table T3. Measurements made by wireline tool strings.

Tool string	Tool	Measurement	Sampling interval (cm)	Approximate vertical resolution (cm)
Triple combination	QSST	Inline check shot	TD – tool string length	
	HNGS	Spectral gamma ray/Total gamma ray	15	51
	APS	Porosity	5 and 15	43
	HLDS/HLDT	Bulk density, photoelectric factor	2.5 and 15	38/46
	DIT	Resistivity, spontaneous potential	15	61
	TAP	Temperature, pressure	1 per second	NA
Formation MicroScanner (FMS)-sonic combination	DSI	Acoustic velocity	15	107
	SGT	Total gamma ray	15	46
	GPIT	Tool orientation	0.25 and 15	NA
	FMS	Microresitivity imaging	0.25	0.5
Well Seismic Tool (stationary)	WST	Sonic traveltime	Variable	NA

Notes: All tool and tool string names presented in this table are trademarks of Schlumberger. For the complete list of acronyms used in the IODP and for additional information consult IODP Downhole Logging Tools at **iodp.ldeo.columbia.edu/TOOLS_LABS/tools.html.** See Table **T4,** for explanation of acronyms used to describe tool string and tools. NA = not applicable.

Table T4. Acronyms and units used for wireline logging tools.

Tool	Output	Tool name/Explanation of output	Unit
APS		Accelerator Porosity Sonde	
	APLC	Near array porosity (limestone calibrated)	%
	SIGF	Formation capture cross section (Σf)	Capture units
	STOF	Tool standoff (distance from borehole wall)	in
DIT		Dual Induction Tool	
	IDPH	Deep induction resistivity	Ωm
	IMPH	Medium induction resistivity	Ωm
	SFLU	Spherically focused resistivity	Ωm
DSI		Dipole Sonic Imager	
	DTCO	Compressional wave delay time (Δt)	ms/ft
	DTSM	Shear wave delay time (Δt)	ms/ft
	DTST	Stoneley wave delay time (Δt)	ms/ft
FMS		Formation MicroScanner	
	C1, C2	Orthogonal hole diameters	inch
	P1AZ	Pad 1 azimuth	Degrees
		Spatially oriented resistivity images of borehole wall	
GPIT		General Purpose Inclinometer Tool	
	DEVI	Hole deviation	Degrees
	HAZI	Hole azimuth	Degrees
	F_x, F_y, F_z	Earth's magnetic field (three orthogonal components)	Oersted
	A_x, A_y, A_z	Acceleration (three orthogonal components)	m/s^2
HLDT		Hostile Environment Litho-Density Tool	
	RHOB	Bulk density (corrected)	g/cm^3
	PEF	Photoelectric effect	b/e^-
	CALI	Caliper (measure of borehole diameter)	inch
	DRHO	Bulk density correction	g/cm^3
HNGS		Hostile Environment Gamma Ray Sonde	
	HSGR	Standard (total) gamma ray	gAPI
	HCGR	Computed gamma ray (HSGR minus uranium contribution)	gAPI
	HFK	Potassium	wt%
	HTHO	Thorium	ppm
	HURA	Uranium	ppm
QSST		Inline Check shot Tool	
SGT		Scintillation Gamma Ray Tool	
	ECGR	Environmentally corrected gamma ray	gAPI
TAP		Temperature/Acceleration/Pressure tool	°C, m/s^2, psi
WST		Well Seismic Tool	
		Acoustic arrival times	ms

Notes: All tool and tool string names (except the TAP and MGT) are trademarks of Schlumberger. For the complete list of acronyms used in the IODP and for additional information about tool physics and use consult IODP Downhole Logging Tools at **iodp.ldeo.columbia.edu/TOOLS_LABS/tools.html.**